Credal Deep Ensembles for Uncertainty Quantification

Kaizheng Wang[1,4,*] **Fabio Cuzzolin**[3] **Shireen Kudukkil Manchingal**[3]
Keivan Shariatmadar[2,4] **David Moens**[2,4] **Hans Hallez**[1]
[1]KU Leuven, Department of Computer Science, DistriNet
[2]KU Leuven, Department of Mechanical Engineering, LMSD
[3]Oxford Brookes University, Visual Artificial Intelligence Laboratory
[4]Flanders Make@KU Leuven
{kaizheng.wang, keivan.shariatmadar, david.moens, hans.hallez}@kuleuven.be
{fabio.cuzzolin, 19185895}@brookes.ac.uk

Abstract

This paper introduces an innovative approach to classification called *Credal Deep Ensembles* (CreDEs), namely, ensembles of novel *Credal-Set Neural Networks* (CreNets). CreNets are trained to predict a lower and an upper probability bound for each class, which, in turn, determine a convex set of probabilities (credal set) on the class set. The training employs a loss inspired by distributionally robust optimization which simulates the potential divergence of the test distribution from the training distribution, in such a way that the width of the predicted probability interval reflects the 'epistemic' uncertainty about the future data distribution. Ensembles can be constructed by training multiple CreNets, each associated with a different random seed, and averaging the outputted intervals. Extensive experiments are conducted on various out-of-distributions (OOD) detection benchmarks (CIFAR10/100 vs SVHN/Tiny-ImageNet, CIFAR10 vs CIFAR10-C, ImageNet vs ImageNet-O) and using different network architectures (ResNet50, VGG16, and ViT Base). Compared to Deep Ensemble baselines, CreDEs demonstrate higher test accuracy, lower expected calibration error, and significantly improved epistemic uncertainty estimation.

1 Introduction

The quantification of the uncertainty associated with neural network predictions has recently attracted increasing attention, to enhance the reliability and robustness of neural networks. Researchers agree to distinguish *aleatory uncertainty* (AU) from *epistemic uncertainty* (EU): the former arises from the inherent randomness, e.g., data noise, and is irreducible. The latter is caused by a lack of knowledge about the process which generates the data, due to the limited availability of training data, and is reducible [1, 36]. Effective EU quantification is beneficial for out-of-distribution (OOD) detection [30, 54] and can contribute to a variety of safety-critical applications, including autonomous driving [21], medical diagnosis [44], flood uncertainty estimation [10], structural health monitoring [72].

In classification, standard neural networks (SNNs) whose predictions amount to single probability distributions are unable to account for epistemic uncertainty, because a single distribution assumes precise knowledge about the dependency between inputs and outputs. To properly capture the EU, the network's outcome needs to express the uncertainty about a prediction's uncertainty itself [35, 62].

The most well-known approach to EU quantification in deep learning leverages Bayesian neural networks (BNNs) [7, 22, 38]. BNNs model network parameters as distributions and thus predict a 'second-order' distribution (i.e., a distribution of distributions) [36], although in practice predictions

*Corresponding author.

38th Conference on Neural Information Processing Systems (NeurIPS 2024).

are often generated by running the network on sample parameters extracted from a posterior. While efficient training techniques (such as sampling [33, 57] and variational inference [7, 22]) have been developed to mitigate their complexity, practical challenges persist for BNNs, including the scaling to large datasets, handling complex network architectures, and real-time applicability [54].

An alternative approach, called Deep Ensembles (DEs), handles uncertainty quantification by aggregating multiple individually-trained SNNs [43], so that predictions amount to finite sets of probability distributions over the classes. DEs, often viewed as an approximation of Bayesian model averaging (BMA) [38], have become a powerful baseline for uncertainty estimation [2, 25, 53, 54, 60]. However, empirical evidence [2] suggests that DEs could yield relatively low-quality estimates of epistemic uncertainty. Further, DEs lack a sound theoretical justification [27, 47].

Credal inference [13, 36, 62] (which predicts convex sets of probability distributions or *credal sets* [46] on the target space) can provide an alternative way of quantifying epistemic uncertainty. Credal representations have been extensively studied within the broader field of machine learning, including, e.g., the naive credal classifier [14], the notion of credal network [13] or credal random forest classification [65]. 'Imprecise' BNNs have been recently introduced which model both network weights and predictions as credal sets [8]. While these models demonstrate robustness in Bayesian sensitivity analysis, their computational complexity is on a par with that of ensembles of BNNs, significantly limiting their practical applicability.

Novelty and Main Contributions. This paper presents an innovative approach to classification tasks called *Credal Deep Ensembles* (CreDEs), ensembles of novel *Credal-Set Neural Networks* (CreNets), aiming to improve EU quantification in the framework of credal inference. At the cost of merely doubling the number of output nodes compared to classical SNNs, CreNets are trained to predict a lower and an upper probability bound for each class rather than a single probability value. Such probability intervals over classes thus efficiently determine a prediction in the form of a credal set. The training strategy is inspired by Distributionally Robust Optimization [42, 55, 61], which simulates the potential divergence of the test distribution from the training distribution. As a result, the width of the predicted probability interval reflects the 'epistemic' uncertainty about the future data distribution. Adopting an ensemble strategy, CreDEs derive the final prediction by averaging the probability intervals outputted by the members of the ensemble. A conceptual comparison between CreDEs and DEs is illustrated in Figure 1.

Extensive experimental validation is conducted on several OOD detection benchmarks, including CIFAR10/100 (ID) vs SVHN/Tiny-ImageNet (OOD), CIFAR10 (ID) vs CIFAR10-C (OOD), ImageNet (ID) vs ImageNet-O (OOD), and across different network architectures: ResNet50, VGG16 and Visual Transformer Base (ViT Base). Compared to traditional Deep Ensembles, our CreDEs achieve *higher test accuracy* and *lower expected calibration error* (ECE) on ID samples, and *significantly improve the quality of EU estimation*.

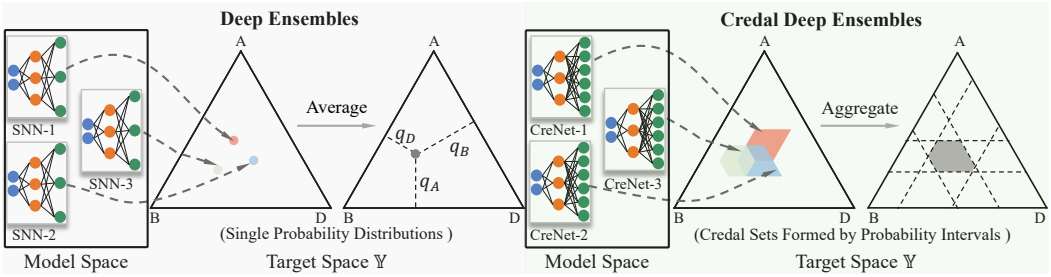

Figure 1: Comparison between the proposed Credal Deep Ensembles and traditional Deep Ensembles. The former aggregate a collection of credal set predictions from CreNets as the final (credal) prediction, whereas the latter average a set of single probability distributions from standard SNNs as the outcome. E.g., in the probability simplex [16] associated with the target space $\mathbb{Y} = \{A, B, D\}$ (the triangle in the figure), a probability vector (q_A, q_B, q_D) is represented as a single point. For each CreNet, the predicted lower and upper probabilities of each class act as constraints (parallel lines) which determine a credal prediction (in gray). Single credal predictions are aggregated as in Sec. 2.4.

Related Work Besides BNNs, DEs, and credal inference, other 'second-order' uncertainty estimation approaches exist, such as Dirichlet-based methods [9, 48, 49, 50, 63], in which predictions are represented as Dirichlet distributions. One significant challenge for the latter is the absence of ground

truth labels. Although various loss functions have been proposed, these models' performance often diverges from theoretical EU assumptions [71]. Another rationale for the exclusion of Dirichlet-based approaches as baselines for our CreDE work is that such models often necessitate the inclusion of OOD data during training [48, 49, 56]. This challenges their practical adaptability, as it cannot guarantee their robustness against other forms of 'unseen' OOD data [71]. Moreover, a recent study [39] has shown that these methods often fail to capture the EU properly, making the resulting measures difficult to interpret quantitatively.

Paper Outline The remainder of this paper is structured as follows. Sec. 2 presents our CreNets and CreDEs in full detail. Sec. 3 describes the experimental validations and results. Sec. 4 summarizes our conclusions and future work. Appendices report mathematical proofs in §A, additional experiments in §B, implementation details in §C, the analysis of alternative ensemble strategies for CreDEs in §D, and further discussion on future work in §E (including achieving statistical guarantees using conformal learning and the framework's extension to regression), respectively.

2 Approach

The proposed Credal-Set Neural Network architecture and forward propagation are introduced in Sec. 2.1. CreNets' training procedure is discussed in Sec. 2.2. The class prediction and uncertainty quantification are discussed in Sec. 2.3. Credal Deep Ensembles are presented in Sec. 2.4.

2.1 Credal-Set Neural Networks

Architecturally, our CreNet design focuses only on the final classification layers, and can therefore be applied on top of any representation layers of neural network models. The final layers of a CreNet (Figure 2) first output a deterministic interval for each class, using for each class an output node associated with the interval midpoint m and one associated with its half-length h, respectively (a total of $2C$ nodes for C classes). Let $\boldsymbol{z}$ be the input vector to the final layer. CreNets compute $\boldsymbol{m}$ and $\boldsymbol{h}$ (the vectors collecting interval midpoints and half-lengths for all classes) as:

$$\begin{aligned} \boldsymbol{m} &= g(\mathbf{W}_{1:C} \cdot \boldsymbol{z} + \boldsymbol{b}_{1:C}) \\ \boldsymbol{h} &= \zeta(\mathbf{W}_{C+1:2C} \cdot \boldsymbol{z} + \boldsymbol{b}_{C+1:2C}), \end{aligned} \tag{1}$$

where $\mathbf{W}_{1:C}, \boldsymbol{b}_{1:C}, \mathbf{W}_{C+1:2C}, \boldsymbol{b}_{C+1:2C}$ are the weights and biases associated with the first C and the remaining C nodes, respectively. Here $g(\cdot)$ is an arbitrary activation function and $\zeta(\cdot)$ denotes the Softplus function [79] that ensures the non-negativity of $\boldsymbol{h}$.

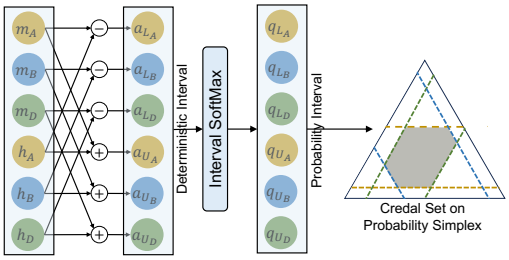

Figure 2: CreNet final layer structure for three classes.

The deterministic intervals associated with all classes, denoted as $[\boldsymbol{a}_L, \boldsymbol{a}_U] := \{[a_{L_i}, a_{U_i}]\}_{i=1}^{C}$, can then be obtained as $[\boldsymbol{a}_L, \boldsymbol{a}_U] = [\boldsymbol{m} - \boldsymbol{h}, \boldsymbol{m} + \boldsymbol{h}]$.

A proper mapping from such deterministic intervals $[\boldsymbol{a}_L, \boldsymbol{a}_U]$ to a collection of probability intervals $[\boldsymbol{q}_L, \boldsymbol{q}_U] := \{[q_{L_i}, q_{U_i}]\}_{i=1}^{C}$ for each class needs to ensure that $[\boldsymbol{q}_L, \boldsymbol{q}_U]$ satisfies the conditions:

$$q_{L\,i} \leq q_{U\,i} \;\forall i = 1, ..., C \quad \text{and} \quad \textstyle\sum_{i=1}^{C} q_{L_i} \leq 1 \leq \sum_{i=1}^{C} q_{U_i}. \tag{2}$$

The former condition guarantees a proper $[q_{L_i}, q_{U_i}]$ for each class. The latter enables the resulting collection of probability intervals to determine a non-empty credal set, $\mathbb{Q}$, as follows [52]:

$$\mathbb{Q} = \{\boldsymbol{q} \,|\, q_i \in [q_{L_i}, q_{U_i}]; \textstyle\sum_{i=1}^{C} q_i = 1\}. \tag{3}$$

The probability vectors in $\mathbb{Q}$ meet the normalization condition, and their probability value per class is constrained by the probability intervals (Eq. (2)).

Traditional SoftMax activation cannot ensure that the convexity conditions in Eq. (2) are met when computing $[\boldsymbol{q}_L, \boldsymbol{q}_U]$ using $\boldsymbol{q}_L = \mathrm{SoftMax}(\boldsymbol{a}_L)$ and $\boldsymbol{q}_U = \mathrm{SoftMax}(\boldsymbol{a}_U)$, respectively. A toy example

is given in Appendix §A. Therefore, we employ Interval SoftMax activation as proposed in [75] to compute $[\boldsymbol{q}_L, \boldsymbol{q}_U]$ from $[\boldsymbol{a}_L, \boldsymbol{a}_U]$, as follows:

$$q_{Li} = \frac{\exp(a_{L_i})}{\exp(a_{L_i}) + \sum_{k \neq i} \exp(\frac{a_{U_k} + a_{L_k}}{2})}, \; q_{Ui} = \frac{\exp(a_{U_i})}{\exp(a_{U_i}) + \sum_{k \neq i} \exp(\frac{a_{U_k} + a_{L_k}}{2})}, \tag{4}$$

where q_{L_i} and q_{U_i} are the lower and upper probability bound for the i^{th} class, respectively. As proven in Appendix §A, the probability intervals generated by the Interval SoftMax duly satisfy Eq. (2).

2.2 Training Procedure

The rationale for the training of a CreNet is for the predicted lower and upper bounds (Eq. (4)) to the probability of the classes, $\boldsymbol{q}_L$ and $\boldsymbol{q}_U$, to express the epistemic uncertainty (induced by the limited size and variability of the training set) about how different the distribution of future test data may be from that of the training data.

To this extent, we designed a composite loss function with two components: one, which applies classical cross entropy to the upper probability vector, encourages the latter to optimistically assume that test data distribution will be similar. The other, inspired by Distributionally Robust Optimization (DRO) [42, 55, 61], pushes the lower probability to reflect a 'pessimistic' stance on future distributional divergence. The width of the resulting interval will thus reflect the epistemic uncertainty associated with the prediction.

We first contrast the classical training strategy with that of Distributionally Robust Optimization in Sec. 2.2.1. We then delve into the design and implementation of our CreNet loss in Sec. 2.2.2.

2.2.1 Classical and DRO Training Strategy

Vanilla Strategy Given a training set $\mathbb{D} = \{\boldsymbol{x}_n, \boldsymbol{t}_n\}_{n=1}^N$, the conventional neural network training process aims to solve the following optimization problem

$$\underset{\boldsymbol{\theta} \in \Theta}{\text{minimize}} \left\{ \frac{1}{N} \sum\nolimits_{n=1}^{N} \mathcal{L}((\boldsymbol{x}_n, \boldsymbol{t}_n), \boldsymbol{\theta}) \right\}, \tag{5}$$

where $\boldsymbol{\theta}$ denotes the model's trainable parameters in the space Θ and $\mathcal{L}$ denotes an arbitrary loss function. The underlying assumption is that the training and test distributions are identical. As a result, the trained network serves as an empirical risk minimizer [36]. However, this ideal assumption often results in over-optimistic predictions because the test observations may, in practice, significantly differ from the training data [34].

DRO Strategy In contrast to the vanilla strategy, the objective of DRO [6, 20] is to minimize the worst-case expected risk ($R(\boldsymbol{\theta})$) over an uncertain set of distributions $\mathcal{U}$, as follows:

$$\underset{\boldsymbol{\theta} \in \Theta}{\text{minimize}} \left\{ R(\boldsymbol{\theta}) \doteq \sup_{U \in \mathcal{U}} \mathbb{E}_{(\boldsymbol{x}, \boldsymbol{t}) \sim U} \mathcal{L}((\boldsymbol{x}, \boldsymbol{t}), \boldsymbol{\theta}) \right\}, \tag{6}$$

in which $\mathbb{E}$ is the expectation operation. In practice, a *group DRO* setting [59] is adopted in which the training distribution P is assumed to be a mixture of m groups P_g, indexed by $g \in \mathcal{G} = \{1, 2, ..., m\}$. Because the optimum of a linear program is attained at a vertex, the worst-case risk in Eq. (6) is equivalent to a maximum over the expected loss of each group, as follows:

$$R(\theta) = \underset{g \in \mathcal{G}}{\text{maximize}} \, \mathbb{E}_{(\boldsymbol{x}, \boldsymbol{t}) \sim P_g} \mathcal{L}((\boldsymbol{x}, \boldsymbol{t}), \boldsymbol{\theta}). \tag{7}$$

In practice, the group DRO model minimizes the empirical worst-group risk $\hat{R}(\theta)$, namely:

$$\underset{\boldsymbol{\theta} \in \Theta}{\text{minimize}} \left\{ \hat{R}(\boldsymbol{\theta}) \doteq \underset{g \in \mathcal{G}}{\text{maximize}} \, \mathbb{E}_{(\boldsymbol{x}, \boldsymbol{t}) \sim \hat{P}_g} \mathcal{L}((\boldsymbol{x}, \boldsymbol{t}), \boldsymbol{\theta}) \right\}, \tag{8}$$

where $\hat{P}_g$ is the empirical distribution of the g-th group of training points. Therefore, group DRO learns models with good worst-group training loss across groups [59]. One special form of *group DRO* is *adversarially reweighted learning* [42], which consists of a minimax game between a learner and adversary. The learner optimizes for the main classification task and aims to learn the best

parameters $\boldsymbol{\theta}$ that minimize the expected loss. In contrast, the adversary maximizes the expected loss by making an adversarial assignment of weights w_n, collected in a vector $\boldsymbol{w}$. Consequently, the training optimization problem assumes the form

$$\underset{\boldsymbol{\theta}\in\Theta}{\text{minimize}} \left\{ \underset{\boldsymbol{w}\in\mathbb{S}}{\text{maximize}} \frac{1}{N} \sum\nolimits_{n=1}^{N} w_n \cdot \mathcal{L}((\boldsymbol{x}_n, \boldsymbol{t}_n), \boldsymbol{\theta}) \right\}, \tag{9}$$

where the set $\mathbb{S}$ of weight vectors varies across different implementations [42, 55, 61].

2.2.2 CreNet Loss Design and Implementation

Design As anticipated, the CreNet training process applies the vanilla training strategy to the upper probability prediction vector $\boldsymbol{q}_U$ (Eq. (5)), and the DRO strategy to the lower probability prediction $\boldsymbol{q}_L$ (Eq. (9)). The resulting overall loss function has a composite structure

$$\mathcal{L}_{\text{CreNet}} := \underbrace{\frac{1}{N}\sum\nolimits_{n=1}^{N} \text{CE}(\boldsymbol{q}_{U_n}, \boldsymbol{t}_n)}_{\text{Vanilla Component}} + \underbrace{\underset{\boldsymbol{w}\in\mathbb{S}}{\text{maximize}} \frac{1}{N}\sum\nolimits_{n=1}^{N} w_n \cdot \text{CE}(\boldsymbol{q}_{L_n}, \boldsymbol{t}_n)}_{\text{DRO Component}}, \tag{10}$$

where CE denotes the classical cross-entropy loss function used in classification. Given a predicted discrete probability vector $\boldsymbol{q}$ and the ground-truth label $\boldsymbol{t}$, CE is defined as: $\text{CE} := -\sum_k^C t_k \cdot \log_2 q_k$. The vanilla component is applied to the upper probability vector $\boldsymbol{q}_U$ because such a loss takes the training distribution at face value and is thus more likely to encourage 'optimistic' (overconfident) or 'upper bound' predictions for the class scores. The DRO component is computed on the lower probability vectors $\boldsymbol{q}_L$, as it weighs training outliers to simulate future differences in data distribution at test time, encouraging 'pessimistic' or 'lower bound' class score predictions. Thus, the width of the resulting probability interval will reflect the uncertainty associated with the model's ignorance of how much the future test distribution will differ from the train distribution, using the boundary/outlier cases observed at training time to guess what the uncertainty on future test cases will be.

Cross-Entropy of Lower/Upper Probability Vectors Please note that in Eq. (10), the CE is applied to lower/upper probability vectors, which are not (normalized) probability vectors. However, as the ground truth (label) vector $\boldsymbol{t}$ equals 1 for the true class j^* and 0 for all the other elements, calculating $\text{CE}(\boldsymbol{q}, \boldsymbol{t})$ for any predicted probability vector $\boldsymbol{q}$ reduces to $-\log_2 q(j^*)$. Consequently, all probability vectors with the same component for the true class will generate the same CE for that sample.

The consequence for CreNet training is that feeding a lower (upper) probability vector $\boldsymbol{q}_L$ ($\boldsymbol{q}_U$) to Eq. (10) is equivalent to computing the CE with *any one* of the probability vectors in the credal prediction (Eq. (3)) whose probability for the true class j^* equals the lower (upper) probability value there. It can be shown that these form one of the 'faces' of the boundary of the credal set.

Importantly, because of the functional structure of Interval SoftMax activation (Eq. (4)), upper and lower probability vectors are not computed independently, but are correlated. Thus, they are minimized together via the total loss (Eq. (10)), with the DRO component also influencing the upper probability $\boldsymbol{q}_U$, driving the solution away from the trivial one (all-ones upper probability vectors).

Implementation As the $\mathbb{S}$ of weight vectors in Eq. (10) varies across different implementations [42, 55, 61] and estimating $\boldsymbol{w}$ in Eq. (10) is not straightforward when using batch-wise training [34], we resort to a simpler heuristic proposed by [34]. For each training batch, only the $\delta \in [0.5, 1)$ portion of samples with the highest cross-entropy with the lower probability vector ($\text{CE}(\boldsymbol{q}_{L_n}, \boldsymbol{t}_n)$) are selected to compute the DRO component of the loss. As a result, $w_n > 1$ is implicitly set in Eq. (10) for selected samples while $w_n = 0$ for deselected samples.

The underlying rationale is the following. Within a batch of samples, those instances that demonstrate high losses are identified as 'hard-to-learn' samples, essentially representing the 'minority group' within a training dataset [34]. Setting a value δ thus identifies what fraction of the training points is chosen to represent potential future domain shifts at test time. A smaller δ signifies a more cautious approach, in which even a few training outliers can indicate future challenges.

The lower bound to the design range for δ is 0.5 because we empirically observed that values of $\delta < 0.5$ may destabilize the training process, as a too-large averaged loss is returned for backpropagation. When δ approaches 1, the data distribution of the samples considered by the vanilla and the DRO components of the loss becomes similar, implicitly assuming a less pronounced divergence between train and test distributions. The corresponding predicted probability intervals become narrower. If δ

were theoretically set to 1, all samples would be selected for backpropagation, implying that $w_n = 1$ for any n in Eq. (10). Consequently, the loss in Eq. (10) would be the sum of the vanilla component on $\boldsymbol{q}_U$ and the vanilla component on $\boldsymbol{q}_L$. Empirically, we observed that this leads to a collapse of the upper and lower probability bounds to single values.

The implementation of the CreNet training procedure is shown in Algorithm 1.

Algorithm 1 CreNet Training Procedure

Input: Training dataset $\mathbb{D} = \{\boldsymbol{x}_n, \boldsymbol{t}_n\}_{n=1}^{N}$; Portion of samples per batch $\delta \in [0.5, 1)$; Batch size η
while *enable training* **do**
1. Compute CE$(\boldsymbol{q}_{U_n}, \boldsymbol{t}_n)$ and CE$(\boldsymbol{q}_{L_n}, \boldsymbol{t}_n)$ for each sample
2. Sort the sample indices $(m_1, ..., m_\eta)$ in descending order of CE$(\boldsymbol{q}_{L_n}, \boldsymbol{t}_n)$
3. Define $\eta_\delta = \lfloor \delta \eta \rfloor$
4. Minimize $\mathcal{L}_{\text{CreNet}} = \frac{1}{\eta} \sum_{n=1}^{\eta} \text{CE}(\boldsymbol{q}_{U_n}, \boldsymbol{t}_n) + \frac{1}{\eta_\delta} \sum_{j=1}^{\eta_\delta} \text{CE}(\boldsymbol{q}_{L_{m_j}}, \boldsymbol{t}_{m_j})$
end while

2.3 Class Prediction and Uncertainty Quantification

Class Prediction For the class prediction we employ the 'maximin' and 'maximax' criteria [66]:

$$\hat{i}_{\text{min}} := \underset{i}{\text{argmax}}\, q^*_{L_i}; \quad \hat{i}_{\text{max}} := \underset{i}{\text{argmax}}\, q^*_{U_i}, \tag{11}$$

which output (respectively) the class indices with the highest lower and upper reachable probability ($q^*_{L_i}$ and $q^*_{U_i}$) within the same credal set induced by the predicted lower and upper probabilities q_{L_i}, q_{U_i}. Figure 3 illustrates how the lower and upper probabilities q_{L_i}, q_{U_i} that determine the credal set $\mathbb{Q}$ may differ from the probabilities $q^*_{L_i}$ and $q^*_{U_i}$ *actually reachable* for each class within $\mathbb{Q}$. The reachable lower and upper probabilities for class i can be easily obtained as follows [17]:

$$q^*_{U_i} = \min\left(q_{U_i}, 1 - \sum_{j \neq i} q_{L_j}\right), q^*_{L_i} = \max\left(q_{L_i}, 1 - \sum_{j \neq i} q_{U_j}\right). \tag{12}$$

Uncertainty Quantification Given a credal set prediction, upper and lower entropies generalizing Shannon's entropy, denoted as $\overline{H}(\mathbb{Q})$ and $\underline{H}(\mathbb{Q})$, can be defined which may serve as measures for TU and AU, respectively [3, 36].

Computing $\overline{H}(\mathbb{Q})$ boils down to solving the following optimization problem:

$$\overline{H}(\mathbb{Q}) = \text{maximize} \sum_{i=1}^{C} -q_i \cdot \log_2 q_i \quad \text{s.t.} \quad q^*_{L_i} \leq q_i \leq q^*_{U_i} \forall i \;\text{ and }\; \sum_{i=1}^{C} q_i = 1. \tag{13}$$

This seeks the highest entropy value of a probability distribution within the predicted credal set $\mathbb{Q}$. $\underline{H}(\mathbb{Q})$, for which maximize is replaced by minimize, searches for the minimal such entropy. Such optimization problems can be addressed using a standard solver, e.g., the SciPy optimization package [73]. Epistemic uncertainty can then be quantified as $\overline{H}(\mathbb{Q}) - \underline{H}(\mathbb{Q})$ [36].

Computational Complexity Reduction To reduce the computational complexity of Eq. (13) for a large value of C (e.g., $C = 1000$), we propose an original approach called *Probability Interval Dimension Reduction* (PIDR) in Algorithm 2. This method first identifies the $K-1$ classes with the highest lower probability values, then merges the remaining elements into a single class with the associated upper and lower probability calculated using Eq. (12). Consequently, the dimension of the probability interval is reduced from C to K.

2.4 Credal Deep Ensembles

Inspired by conventional DEs [43], the final step of our approach is to introduce *Credal Deep Ensembles* (CreDEs). CreDEs aggregate M individually trained CreNets and predict the aggregated probability intervals, denoted as $[\tilde{\boldsymbol{q}}^*_L, \tilde{\boldsymbol{q}}^*_U]$, as follows:

$$\tilde{\boldsymbol{q}}^*_L = \frac{1}{M} \sum_{m=1}^{M} \boldsymbol{q}^*_{L_m}, \quad \tilde{\boldsymbol{q}}^*_U = \frac{1}{M} \sum_{m=1}^{M} \boldsymbol{q}^*_{U_m}, \tag{14}$$

where $[\boldsymbol{q}^*_{L_m}, \boldsymbol{q}^*_{U_m}]$ is the set of reachable probability intervals predicted by the m-th CreNet. Eq. (20) in Appendix D proves that $[\tilde{\boldsymbol{q}}^*_L, \tilde{\boldsymbol{q}}^*_U]$ satisfies the convexity condition in Eq. (2) for constructing a

Algorithm 2 Probability Interval Dimension Reduction Algorithm

Input: $[\boldsymbol{q}_L^*, \boldsymbol{q}_U^*]$; Chosen number of classes K
Output: Reduced-dimensional probability intervals $[\boldsymbol{r}_L, \boldsymbol{r}_U]$
1. Index vector of $\boldsymbol{q}_L^*$ in descending order: $\boldsymbol{l} \leftarrow \text{argsort}(\boldsymbol{q}_L^*)$
2. Define the upper and lower probability per selected class:
$r_{L_j} \leftarrow q^*_{L_{l_j}}, r_{U_j} \leftarrow q^*_{U_{l_j}}$ for $j = 1, ..., K-1$
3. Define upper and lower probability for deselected classes:
$r_{L_K} \leftarrow \max(1 - \sum_{i=l_K}^{l_C} q^*_{U_i}, \sum_{j=1}^{K-1} r_{L_j})$;
$r_{U_K} \leftarrow \min(1 - \sum_{i=l_K}^{l_C} q^*_{L_i}, \sum_{j=1}^{K-1} r_{U_j})$

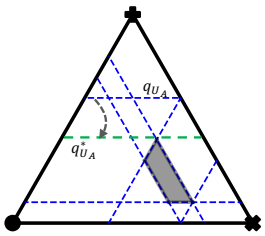

Figure 3: If intervals are redundant, some of the (e.g.) upper probabilities q_{U_A} may not be actually reachable in the credal set that results from the intersection of all interval constraints.

non-empty credal set. Therefore, class prediction and uncertainty estimation as described in Sec. 2.3 apply to CreDEs. We discuss the rationale for averaging strategy and the alternative ensemble approaches for CreDEs in Appendix §D.

3 Experimental Validation

Setup We assessed CreDEs through OOD detection benchmarks across various dataset pairings (ID vs OOD samples), including CIFAR10 [41]/CIFAR100 [40] vs SVHN [31]/Tiny-ImageNet [45], CIFAR10 vs CIFAR10-C [29], ImageNet [18] vs ImageNet-O [31]. We trained 15 CreNets (using $\delta = 0.5$) and SNNs on the ResNet50 architecture [28] starting from different random seeds, using the training set as per the ID dataset in the pair. Following this, we constructed 15 different CreDEs and DEs, respectively, by randomly selecting five members from the pool of 15 trained models. The same ensemble member lists are used for both DEs and CreDEs, with each ensemble strictly guaranteed to be distinct. More details are given in Appendix §C. Codes are available at `https://gitlab.kuleuven.be/m-group-campus-brugge/distrinet_public/credal-deep-ensembles.git`.

Uncertainty Quantification in DEs Total uncertainty (TU) can be quantified in DEs via the Shannon entropy (H) of the averaged predicted distribution. The AU, on the other hand, can be obtained by averaging the entropies of the predictions of each ensemble member [2, 36]. Namely,

$$\text{TU} := H(\tilde{\boldsymbol{q}}) = H(\tfrac{1}{M} \textstyle\sum_{m=1}^{M} \boldsymbol{q}_m), \quad \text{AU} := \tilde{H}(\boldsymbol{q}) = \tfrac{1}{M} \textstyle\sum_{m=1}^{M} H(\boldsymbol{q}_m), \tag{15}$$

where M is the number of networks, $\tilde{\boldsymbol{q}}$ and $\boldsymbol{q}_m$ denote the average probability vector and the single probability vector of the m-th SNN model, respectively. The level of epistemic uncertainty, representing an approximation of mutual information [36], can be obtained as $\text{EU} := H(\tilde{\boldsymbol{q}}) - \tilde{H}(\boldsymbol{q})$.

Test Accuracy and ECE on ID Samples We evaluated the test accuracy and expected calibration error (ECE) [24, 58] of CreDEs-5 and DEs-5 on the test set of each ID dataset. A lower ECE value signifies a closer alignment between the model's confidence scores and the true probabilities of the events. Since ECE is designed for a singular probability vector, we implemented a compromise calculation as follows. Suppose our model predicts the class indices k and j when using the $\hat{i}_{\text{min}}$ and $\hat{i}_{\text{max}}$ criteria, respectively, ECE values are then computed based on the associated lower $q^*_{L_k}$ and upper $q^*_{U_j}$ reachable probabilities in the credal set.

Table 1 reports the test accuracy and ECE for DEs-5 and CreDEs-5 on the various datasets, indicating that our CreDEs-5 achieved *higher test accuracy* and *lower ECE* on ID samples. Note that employing the $\hat{i}_{\text{min}}$ prediction showed higher ECE on the challenging ImageNet dataset. This is likely because the strategy, selecting the class with the highest lower reachable probability, is a conservative one.

Table 1: Test accuracy (%, ↑) and ECE (↓) of DEs-5 and CreDEs-5 using CIFAR10, CIFAR100, and ImageNet as ID datasets over 15 runs. The better performance is marked in bold.

		CIFAR10		CIFAR100		ImageNet	
		Test Accuracy	ECE	Test Accuracy	ECE	Test Accuracy	ECE
DEs-5		93.32±0.13	0.0131±0.0010	75.80±0.28	0.0392±0.0027	77.92±0.02	0.2415±0.0009
CreDEs-5 (Ours)	$\hat{i}_{\text{min}}$	**93.75±0.11**	**0.0092±0.0016**	**79.54±0.21**	**0.0366±0.0025**	**78.41±0.02**	0.5930±0.0006
	$\hat{i}_{\text{max}}$	**93.74±0.11**	**0.0108±0.0017**	**79.65±0.19**	**0.0268±0.0023**	**78.51±0.02**	**0.1685±0.0004**

Table 2: OOD detection AUROC and AUPRC performance (%, ↑) between CreDEs-5 and DEs-5 based on ResNet50 using EU as uncertainty metrics on CIFAR10/100 vs. SVHN/Tiny-ImageNet and ImageNet vs. ImageNet-O. Results are averaged over 15 runs. Best results in bold.

ID Samples		CIFAR10				CIFAR100				ImageNet	
OOD Samples		SVHN		Tiny-ImageNet		SVHN		Tiny-ImageNet		ImageNet-O	
Performance Indicator		AUROC	AUPRC	AUROC	AUPRC	AUROC	AUPRC	AUROC	AUPRC	AUROC	AUPRC
DEs-5	$H(\tilde{\boldsymbol{q}})-\tilde{H}(\boldsymbol{q})$	89.58±0.93	92.29±1.00	86.87±0.20	83.02±0.16	73.83±1.97	84.96±1.25	78.80±0.20	74.68±0.27	65.03±0.53	62.77±0.38
CreDEs-5	$\overline{H}(\mathbb{Q})-\underline{H}(\mathbb{Q})$	**96.55±0.25**	**98.17±0.17**	**88.10±0.26**	**87.85±0.35**	**78.55±1.15**	**86.57±0.65**	**82.54±0.26**	**77.60±0.44**	**67.82±0.06**	**62.80±0.12**

EU Quantification for OOD Detection It is our hypothesis that OOD data express a higher EU. Hence, we can use a better EU quantification as the means to improve the OOD detection [54]. Thus, superior OOD detection performance provides compelling evidence of enhanced uncertainty estimation quality. For the OOD detection performance assessment, we employed AUROC (Area Under the Receiver Operating Characteristic curve) and AUPRC (Area Under the Precision-Recall curve) scores. AUROC captures true and false positive rates, while AUPRC assesses precision and recall trade-offs, offering valuable insights into model effectiveness across various confidence levels. When calculating $\overline{H}(\mathbb{Q})$ and $\underline{H}(\mathbb{Q})$ in the ImageNet vs ImageNet-O experiment, we employed our PIDR Algorithm 2 with $K = 20$. Table 2 reports the OOD detection performance of CreDEs-5 and DEs-5 in the CIFAR10/CIFAR100 vs SVHN/Tiny-ImageNet, and ImageNet vs ImageNet-O settings. As the CIFAR10-C dataset contemplates data from CIFAR10 corrupted in 15 distinct ways, each with 5 different intensities, Figure 4 presents averaged AUROC and AUPRC scores for OOD detection on CIFAR10 vs CIFAR10-C across types of corruption, against the intensity of corruption. Table 2 and Figure 4 confirm CreDEs-5's superior OOD detection performance over DEs-5. This indicates the effectiveness of CreDEs in improving the EU quantification quality, using $\overline{H}(\mathbb{Q})-\underline{H}(\mathbb{Q})$ as the uncertainty measures.

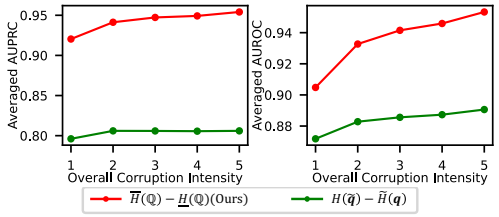

Figure 4: OOD detection (CIFAR10 vs CIFAR10-C) over increased corruption intensity.

Qualitative Evaluation Due to the high dimensionality, visualizing or directly computing the size of the credal set becomes challenging as C increases. Consequently, we indirectly evaluate whether our CreDEs consistently generate nearly Dirac credal sets as predictions through the maximum attainable upper bound probability of the prediction. The closer this probability is to 1, the more it approximates a Dirac credal set. Figure 5 shows the results of ResNet50-based CreDEs-5 for the CIFAR10, SVHN, and Tiny-ImageNet datasets. It verifies that our method does not consistently generate nearly Dirac credal sets, especially for OOD samples. For CIFAR10, a substantial proportion of (but not all) the credal sets are quasi-Dirac. This observation is reasonable as it is consistent with the high test accuracy of CreDEs and the low ECE reported in Table 1.

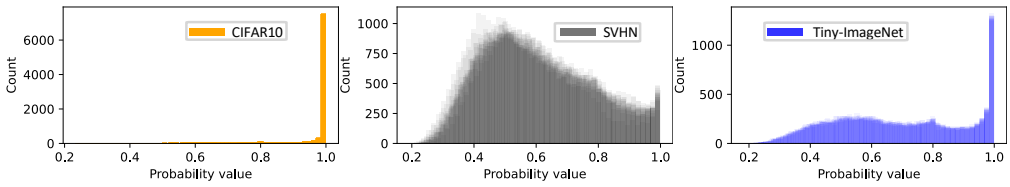

Figure 5: Maximum reachable upper probability $\max(q^*_{U_1}, ..., q^*_{U_C})$ per sample from 15 runs.

Additionally, Figure 6 shows the reliability diagram[24] of the ResNet50-based DEs-5 and CreDEs-5 on the CIFAR10 dataset, demonstrating better calibration performance of our CreDEs. Figure 7 showcases the EU estimation plots for these models. Although the EU estimates for DEs-5 and CreDEs-5 are not directly comparable due to differing representations, CreDEs-5 demonstrates significantly higher EU estimates for OOD samples, as observed qualitatively.

Ablation Study on Various Network Architectures We also performed an ablation study on network backbones different from ResNet50, including VGG16 [67] and Vision Transformer Base (ViT Base)

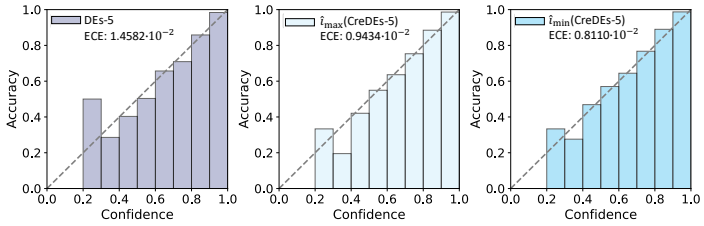

Figure 6: Reliability diagram of ResNet50-based DEs-5 and CreDEs-5 (using $\hat{i}_{min}$ and $\hat{i}_{max}$, respectively) on CIFAR10.

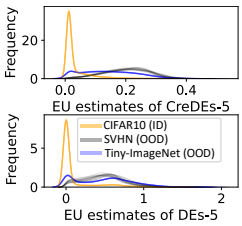

Figure 7: EU estimates comparison of ResNet50-based models.

[77]. Table 3 reports the test accuracy and ECE of CreDEs-5 and DEs-5 on the CIFAR10 test set (representing ID samples) and the OOD detection performance on CIFAR10 vs SVHN/Tiny-ImageNet. Figure 8 compares OOD detection performance in the CIFAR10 vs CIFAR10-C setting against the intensity of corruption, using both AUPRC and AUROC as metrics. The results consistently demonstrate that CreDEs achieve *higher test accuracy*, *lower ECE*, and *significantly improved epistemic uncertainty estimation*, leading to enhanced OOD detection performance.

Table 3: Test accuracy (%, ↑) and ECE (↓) of DEs-5 and CreDEs-5 on CIFAR10 as ID dataset (left). AUROC and AUPRC scores (%, ↑) for OOD detection on CIFAR10 vs SVHN/Tiny-ImageNet (right). Results averaged over 15 runs. The Best results are in bold.

			CIFAR10 (ID)			CIFAR10 vs SVHN		CIFAR10 vs Tiny-ImageNet	
			Test Accuracy	ECE		AUROC	AUPRC	AUROC	AUPRC
VGG16	DEs-5		85.53±0.10	0.0815±0.0011	$H(\tilde{\boldsymbol{q}})$–$\tilde{H}(\boldsymbol{q})$	82.19±0.82	87.52±0.81	78.58±0.15	73.28±0.23
	CreDEs-5 (Ours)	$\hat{i}_{\text{min}}$	**87.94±0.11**	**0.0203±0.0014**	$\overline{H}(\mathbb{Q})$–$\underline{H}(\mathbb{Q})$	**87.68±0.73**	**93.47±0.57**	**82.56±0.28**	**80.81±0.52**
		$\hat{i}_{\text{max}}$	**87.92±0.11**	**0.0611±0.0012**					
ViT Base	DEs-5		90.43±0.97	0.0181±0.0019	$H(\tilde{\boldsymbol{q}})$–$\tilde{H}(\boldsymbol{q})$	77.71±1.67	88.73±0.32	82.27±0.79	78.85±0.81
	CreDEs-5 (Ours)	$\hat{i}_{\text{min}}$	**93.60±0.40**	**0.0107±0.0014**	$\overline{H}(\mathbb{Q})$–$\underline{H}(\mathbb{Q})$	**88.57±2.08**	**93.24±1.25**	**88.73±0.32**	**87.84±0.52**
		$\hat{i}_{\text{max}}$	**93.59±0.39**	**0.0104±0.0012**					

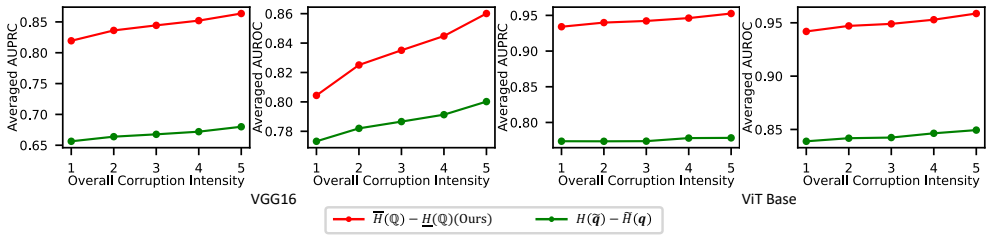

Figure 8: OOD detection on CIFAR10 vs CIFAR10-C against increased corruption intensity, using VGG16 and ViT Base as backbones.

Ablation Study on Hyperparameter δ for CreNet Training In our main evaluation, we set by default $\delta = 0.5$ to reflect a balanced assessment of the train-test divergence and show how such a value allows our model to outperform the baselines. Table 4 reports the test accuracy and OOD detection performance (using EU estimates) of CreDEs-5 under various values of δ. The ablation findings verify the robustness of CreDEs across hyperparameter setups and indicate the $\delta = 0.5$ might be too pessimistic a choice in CIFAR10 settings. Performance peaks at $\delta = 0.875$ in most cases, implying that $\delta = 0.875$ may provide the 'optimal' estimate of how test and train sets diverge for CIFAR10. One possible way to find the 'best' δ in practice is to conduct standard cross-validation on specific test scenarios. However, the method is not particularly sensitive to this hyperparameter. Perspectively, an interesting option, in the presence of multiple datasets (e.g.acquired over time in a continual learning setting), could be applying the DRO loss component to different components of the training set, and assessing the results to robustly select δ.

Table 4: Test accuracy (%, ↑) and OOD detection performance (%, ↑) of CreDEs-5 using various δ. Results are averaged over 15 runs.

δ		0.5	0.625	0.75	0.875	0.9375	0.96875
Test Accuracy (CIFAR10)	$\hat{i}_{\text{max}}$	93.74	94.54	94.47	94.57	93.88	93.99
	$\hat{i}_{\text{min}}$	93.75	94.55	94.47	94.56	93.87	93.99
SVHN (OOD Detection)	AUROC	97.44	97.44	97.92	97.95	97.42	97.51
	AUPRC	93.07	96.34	97.00	96.92	98.79	98.82
Tiny-ImageNet (OOD Detection)	AUROC	88.28	89.01	89.10	89.18	89.85	89.24
	AUPRC	88.13	89.81	89.76	89.72	89.18	89.26

We also report the average EU estimation values of CreDEs-5 for each dataset in Table 5. Increasing the value of δ (i.e., giving less importance to the divergence between test and training

distributions) leads to a decreasing trend in the average EU estimates per dataset (particularly for ID CIFAR10 samples). This aligns with the intuition that, if the model is more uncertain about the divergence of the distributions (smaller δ), it should express a larger EU. Despite smaller uncertainty values at high δ's, the difference between ID and OOD samples remains noticeable. This explains why a δ closer to 1 does not always lead to low-performance OOD detection and why our model's OOD detection performance is robust against the choice of δ.

Table 5: Averaged EU estimates of CreDEs-5 using various δ.

δ	0.5	0.625	0.75	0.875	0.9375	0.96875
CIFAR10	0.3557	0.0611	0.0586	0.0572	0.0222	0.0215
SVHN	1.6093	0.2450	0.2553	0.2593	0.1612	0.1574
Tiny-ImageNet	1.4996	0.2030	0.1957	0.1970	0.1025	0.1005

Model Inference Complexity Table 6 reports the parameter count and inference cost on one NVIDIA A100-SXM4-40GB GPU for a single SNN and CreNet on ImageNet. CreNets show a marginal increase in complexity due to its minor architectural modifications. More discussions on the inference and training complexity are presented in Appendix §C.

Additional Experiments Appendix §B.1 discusses the implementation and performance of EU quantification in CreDEs when using a different uncertainty measure for credal sets (the *generalized Hartley measure* [4, 36]). The results demonstrate that our CreDEs consistently enhance the quality of EU quantification, exhibiting robustness against different measures. Appendix §B.2 reports an ablation study for the hyperparameter K of our PIDR Algorithm 2, which shows the effect of K on CreDEs's uncertainty quantification and time cost. Appendix §B.3 assesses the ability of CreDEs to evaluate *total uncertainty* (TU) (as opposed to EU) in OOD detection, suggesting that our CreDEs also achieve an improved TU estimation, compared to DEs. Appendices §B.4, §B.5, and §B.6 compare the uncertainty quantification abilities of CreDEs versus those of traditional DEs that also apply the DRO strategy, DEs that apply the 'product of experts' [32] ensemble setting, several BNN baselines, respectively. CreDEs continue to demonstrate superior performance in uncertainty estimation. Appendix §B.7 assess CreDEs in a case study involving active learning [23, 54]. All these additional experiments demonstrate that our CreDEs deliver improved uncertainty quantification.

Table 6: Model complexity of a ResNet50-based SNN and CreNet on ImageNet dataset.

Model	Parameters (million)	Inference time per sample (ms)
SNN vs CreNet	25.557 vs 27.606	5.5±0.2 vs 5.7±0.3

4 Conclusion

Conclusion In this paper, we introduced a novel *Credal-Set Neural Network* (CreNet) for classification tasks. Given any given input instance, CreNet is designed to predict a lower and an upper probability for each class, rather than a single probability value, thus providing an efficient and effective implementation of credal inference. We also proposed *Credal Deep Ensembles* (CreDEs), ensembles of CreNets, which extend the traditional deep ensemble idea to the credal domain. Extensive experimental validation was conducted on several OOD detection benchmarks, and across different network architectures and uncertainty measures. Compared to traditional Deep Ensembles, our CreDEs achieve higher test accuracy and lower ECE on ID samples, while significantly improving the quality of EU and TU estimation, leading in turn to strongly enhanced OOD detection performance. Hence, we believe our work can potentially improve neural network safety and reliability, and have wide applicability to real-world scenarios such as medical image analysis.

Limitation Despite the superior performance of CreDEs, neither traditional DEs nor CreDEs may be desirable when memory usage is stringent and computational resources are limited.

Future Work Three essential objectives of our future research include elaborating on statistical coverage guarantees of our CreDEs (outlined in Appendix §E.2), extending our framework to regression tasks (a roadmap is provided in Appendix §E.3), and assessing our CreDEs alongside other uncertainty-aware models in real-world applications comprehensively, like medical image analysis.

Acknowledgement

We thank the anonymous reviewers for their valuable feedback. This work has received funding from the European Union's Horizon 2020 research and innovation program under grant agreement No. 964505 (E-pi).

References

[1] Moloud Abdar, Farhad Pourpanah, Sadiq Hussain, Dana Rezazadegan, Li Liu, Mohammad Ghavamzadeh, Paul Fieguth, Xiaochun Cao, Abbas Khosravi, U Rajendra Acharya, et al. A review of uncertainty quantification in deep learning: Techniques, applications and challenges. *Information Fusion*, 76:243–297, 2021.

[2] Taiga Abe, Estefany Kelly Buchanan, Geoff Pleiss, Richard Zemel, and John P Cunningham. Deep ensembles work, but are they necessary? *Advances in Neural Information Processing Systems*, 35:33646–33660, 2022.

[3] Joaquín Abellán, George J Klir, and Serafín Moral. Disaggregated total uncertainty measure for credal sets. *International Journal of General Systems*, 35(1):29–44, 2006.

[4] Joaquín Abellán and Serafín Moral. A non-specificity measure for convex sets of probability distributions. *International journal of uncertainty, fuzziness and knowledge-based systems*, 8(03):357–367, 2000.

[5] Tathagata Basu, Matthias CM Troffaes, and Jochen Einbeck. Binary credal classification under sparsity constraints. In *International Conference on Information Processing and Management of Uncertainty in Knowledge-Based Systems*, pages 82–95. Springer, 2020.

[6] Aharon Ben-Tal, Dick Den Hertog, Anja De Waegenaere, Bertrand Melenberg, and Gijs Rennen. Robust solutions of optimization problems affected by uncertain probabilities. *Management Science*, 59(2):341–357, 2013.

[7] Charles Blundell, Julien Cornebise, Koray Kavukcuoglu, and Daan Wierstra. Weight uncertainty in neural network. In *Proceedings of the International Conference on Machine Learning*, pages 1613–1622. PMLR, 2015.

[8] Michele Caprio, Souradeep Dutta, Kuk Jin Jang, Vivian Lin, Radoslav Ivanov, Oleg Sokolsky, and Insup Lee. Imprecise Bayesian neural networks. *arXiv preprint arXiv:2302.09656*, 2023.

[9] Bertrand Charpentier, Daniel Zügner, and Stephan Günnemann. Posterior network: Uncertainty estimation without OOD samples via density-based pseudo-counts. *Advances in neural information processing systems*, 33:1356–1367, 2020.

[10] Priyanka Chaudhary, João P Leitão, Tabea Donauer, Stefano D'Aronco, Nathanaël Perraudin, Guillaume Obozinski, Fernando Perez-Cruz, Konrad Schindler, Jan Dirk Wegner, and Stefania Russo. Flood uncertainty estimation using deep ensembles. *Water*, 14(19):2980, 2022.

[11] David Cohn, Zoubin Ghahramani, and Michael Jordan. Active learning with statistical models. *Advances in neural information processing systems*, 7, 1994.

[12] Giorgio Corani and Alessandro Antonucci. Credal ensembles of classifiers. *Computational statistics & data analysis*, 71:818–831, 2014.

[13] Giorgio Corani, Alessandro Antonucci, and Marco Zaffalon. Bayesian networks with imprecise probabilities: Theory and application to classification. *Data Mining: Foundations and Intelligent Paradigms: Volume 1: Clustering, Association and Classification*, pages 49–93, 2012.

[14] Giorgio Corani and Marco Zaffalon. Learning reliable classifiers from small or incomplete data sets: The naive credal classifier 2. *Journal of Machine Learning Research*, 9(4), 2008.

[15] Fabio Cuzzolin. Credal semantics of bayesian transformations in terms of probability intervals. *IEEE Transactions on Systems, Man, and Cybernetics, Part B (Cybernetics)*, 40(2):421–432, 2009.

[16] Fabio Cuzzolin. *The geometry of uncertainty: The geometry of imprecise probabilities*. Springer Nature, 2020.

[17] Luis M. De Campos, Juan F. Huete, and Serafin Moral. Probability intervals: A tool for uncertain reasoning. *International Journal of Uncertainty, Fuzziness and Knowledge-Based Systems*, 02:167–196, June 1994.

[18] Jia Deng, Wei Dong, Richard Socher, Li-Jia Li, Kai Li, and Li Fei-Fei. Imagenet: A large-scale hierarchical image database. In *2009 IEEE conference on computer vision and pattern recognition*, pages 248–255. Ieee, 2009.

[19] Thierry Denœux. An evidential neural network model for regression based on random fuzzy numbers. In *International Conference on Belief Functions*, pages 57–66. Springer, 2022.

[20] John C Duchi, Peter W Glynn, and Hongseok Namkoong. Statistics of robust optimization: A generalized empirical likelihood approach. *Mathematics of Operations Research*, 46(3):946–969, 2021.

[21] Stanislav Fort and Stanislaw Jastrzebski. Large scale structure of neural network loss landscapes. *Advances in Neural Information Processing Systems*, 32, 2019.

[22] Yarin Gal and Zoubin Ghahramani. Dropout as a Bayesian approximation: Representing model uncertainty in deep learning. In *Proceedings of the International Conference on Machine Learning*, pages 1050–1059. PMLR, 2016.

[23] Yarin Gal, Riashat Islam, and Zoubin Ghahramani. Deep Bayesian active learning with image data. In *International conference on machine learning*, pages 1183–1192. PMLR, 2017.

[24] Chuan Guo, Geoff Pleiss, Yu Sun, and Kilian Q Weinberger. On calibration of modern neural networks. In *International conference on machine learning*, pages 1321–1330. PMLR, 2017.

[25] Fredrik K Gustafsson, Martin Danelljan, and Thomas B Schon. Evaluating scalable Bayesian deep learning methods for robust computer vision. In *Proceedings of the IEEE/CVF conference on computer vision and pattern recognition workshops*, pages 318–319, 2020.

[26] Ralph VL Hartley. Transmission of information 1. *Bell System technical journal*, 7(3):535–563, 1928.

[27] Bobby He, Balaji Lakshminarayanan, and Yee Whye Teh. Bayesian deep ensembles via the neural tangent kernel. *Advances in neural information processing systems*, 33:1010–1022, 2020.

[28] Kaiming He, Xiangyu Zhang, Shaoqing Ren, and Jian Sun. Deep residual learning for image recognition. In *Proceedings of the IEEE conference on computer vision and pattern recognition*, pages 770–778, 2016.

[29] Dan Hendrycks and Thomas Dietterich. Benchmarking neural network robustness to common corruptions and perturbations. *Proceedings of the International Conference on Learning Representations*, 2019.

[30] Dan Hendrycks and Kevin Gimpel. A baseline for detecting misclassified and out-of-distribution examples in neural networks. *arXiv preprint arXiv:1610.02136*, 2016.

[31] Dan Hendrycks, Kevin Zhao, Steven Basart, Jacob Steinhardt, and Dawn Song. Natural adversarial examples. In *Proceedings of the IEEE/CVF Conference on Computer Vision and Pattern Recognition*, pages 15262–15271, 2021.

[32] Geoffrey E. Hinton. Products of experts. In *Proceedings of the Ninth International Conference on Artificial Neural Networks*, 1999.

[33] Matthew D Hoffman, Andrew Gelman, et al. The No-U-Turn sampler: adaptively setting path lengths in Hamiltonian Monte Carlo. *J. Mach. Learn. Res.*, 15(1):1593–1623, 2014.

[34] Zeyi Huang, Haohan Wang, Dong Huang, Yong Jae Lee, and Eric P Xing. The two dimensions of worst-case training and their integrated effect for out-of-domain generalization. In *Proceedings of the IEEE/CVF Conference on Computer Vision and Pattern Recognition*, pages 9631–9641, 2022.

[35] Eyke Hüllermeier, Sébastien Destercke, and Mohammad Hossein Shaker. Quantification of credal uncertainty in machine learning: A critical analysis and empirical comparison. In *Proceedings of the Uncertainty in Artificial Intelligence*, pages 548–557. PMLR, 2022.

[36] Eyke Hüllermeier and Willem Waegeman. Aleatoric and epistemic uncertainty in machine learning: An introduction to concepts and methods. *Machine Learning*, 110(3):457–506, 2021.

[37] Alireza Javanmardi, David Stutz, and Eyke Hüllermeier. Conformalized credal set predictors. *arXiv preprint arXiv:2402.10723*, 2024.

[38] Laurent Valentin Jospin, Hamid Laga, Farid Boussaid, Wray Buntine, and Mohammed Bennamoun. Hands-on Bayesian neural networks—A tutorial for deep learning users. *IEEE Computational Intelligence Magazine*, 17(2):29–48, 2022.

[39] Mira Juergens, Nis Meinert, Viktor Bengs, Eyke Hüllermeier, and Willem Waegeman. Is epistemic uncertainty faithfully represented by evidential deep learning methods? In *Forty-first International Conference on Machine Learning*, 2024.

[40] Alex Krizhevsky. Learning multiple layers of features from tiny images. *University of Toronto*, 05 2012.

[41] Alex Krizhevsky, Vinod Nair, and Geoffrey Hinton. CIFAR-10 (Canadian Institute For Advanced Research). Technical report, CIFAR, 2009.

[42] Preethi Lahoti, Alex Beutel, Jilin Chen, Kang Lee, Flavien Prost, Nithum Thain, Xuezhi Wang, and Ed Chi. Fairness without demographics through adversarially reweighted learning. *Advances in neural information processing systems*, 33:728–740, 2020.

[43] Balaji Lakshminarayanan, Alexander Pritzel, and Charles Blundell. Simple and scalable predictive uncertainty estimation using deep ensembles. *Advances in Neural Information Processing Systems*, 30, 2017.

[44] Antonis Lambrou, Harris Papadopoulos, and Alex Gammerman. Reliable confidence measures for medical diagnosis with evolutionary algorithms. *IEEE Transactions on Information Technology in Biomedicine*, 15(1):93–99, 2010.

[45] Ya Le and Xuan Yang. Tiny imagenet visual recognition challenge. *CS 231N*, 7(7):3, 2015.

[46] Isaac Levi. *The enterprise of knowledge: An essay on knowledge, credal probability, and chance*. MIT press, 1980.

[47] Jeremiah Liu, Zi Lin, Shreyas Padhy, Dustin Tran, Tania Bedrax Weiss, and Balaji Lakshminarayanan. Simple and principled uncertainty estimation with deterministic deep learning via distance awareness. *Advances in Neural Information Processing Systems*, 33:7498–7512, 2020.

[48] Andrey Malinin and Mark Gales. Predictive uncertainty estimation via prior networks. *Advances in neural information processing systems*, 31, 2018.

[49] Andrey Malinin and Mark Gales. Reverse KL-divergence training of prior networks: Improved uncertainty and adversarial robustness. *Advances in Neural Information Processing Systems*, 32, 2019.

[50] Andrey Malinin, Bruno Mlodozeniec, and Mark Gales. Ensemble distribution distillation. In *International Conference on Learning Representations*, 2019.

[51] Dmitry Molchanov, Arsenii Ashukha, and Dmitry Vetrov. Variational dropout sparsifies deep neural networks. In *International conference on machine learning*, pages 2498–2507. PMLR, 2017.

[52] Serafín Moral-García and Joaquín Abellán. Credal sets representable by reachable probability intervals and belief functions. *International Journal of Approximate Reasoning*, 129:84–102, 2021.

[53] Bálint Mucsányi, Michael Kirchhof, and Seong Joon Oh. Benchmarking uncertainty disentanglement: Specialized uncertainties for specialized tasks. *arXiv preprint arXiv:2402.19460*, 2024.

[54] Jishnu Mukhoti, Andreas Kirsch, Joost van Amersfoort, Philip HS Torr, and Yarin Gal. Deep deterministic uncertainty: A new simple baseline. In *Proceedings of the IEEE/CVF Conference on Computer Vision and Pattern Recognition*, pages 24384–24394, 2023.

[55] Junhyun Nam, Hyuntak Cha, Sungsoo Ahn, Jaeho Lee, and Jinwoo Shin. Learning from failure: De-biasing classifier from biased classifier. *Advances in Neural Information Processing Systems*, 33:20673–20684, 2020.

[56] Jay Nandy, Wynne Hsu, and Mong Li Lee. Towards maximizing the representation gap between in-domain & out-of-distribution examples. *Advances in neural information processing systems*, 33:9239–9250, 2020.

[57] Radford M Neal et al. MCMC using Hamiltonian dynamics. *Handbook of Markov Chain Monte Carlo*, 2(11):2, 2011.

[58] Jeremy Nixon, Michael W Dusenberry, Linchuan Zhang, Ghassen Jerfel, and Dustin Tran. Measuring calibration in deep learning. In *CVPR workshops*, volume 2, 2019.

[59] Yonatan Oren, Shiori Sagawa, Tatsunori B Hashimoto, and Percy Liang. Distributionally robust language modeling. *arXiv preprint arXiv:1909.02060*, 2019.

[60] Yaniv Ovadia, Emily Fertig, Jie Ren, Zachary Nado, David Sculley, Sebastian Nowozin, Joshua Dillon, Balaji Lakshminarayanan, and Jasper Snoek. Can you trust your model's uncertainty? evaluating predictive uncertainty under dataset shift. *Advances in neural information processing systems*, 32, 2019.

[61] Shiori Sagawa, Pang Wei Koh, Tatsunori B Hashimoto, and Percy Liang. Distributionally robust neural networks for group shifts: On the importance of regularization for worst-case generalization. *arXiv preprint arXiv:1911.08731*, 2019.

[62] Yusuf Sale, Michele Caprio, and Eyke Höllermeier. Is the volume of a credal set a good measure for epistemic uncertainty? In *Uncertainty in Artificial Intelligence*, pages 1795–1804. PMLR, 2023.

[63] Murat Sensoy, Lance Kaplan, and Melih Kandemir. Evidential deep learning to quantify classification uncertainty. *Advances in neural information processing systems*, 31, 2018.

[64] Glenn Shafer and Vladimir Vovk. A tutorial on Conformal Prediction. *Journal of Machine Learning Research*, 9(3), 2008.

[65] Mohammad Hossein Shaker and Eyke Hüllermeier. Ensemble-based uncertainty quantification: Bayesian versus credal inference. In *PROCEEDINGS 31. WORKSHOP COMPUTATIONAL INTELLIGENCE*, volume 25, page 63, 2021.

[66] Keivan Shariatmadar and Mark Versteyhe. Numerical linear programming under non-probabilistic uncertainty models—interval and fuzzy sets. *International Journal of Uncertainty, Fuzziness and Knowledge-Based Systems*, 28(03):469–495, 2020.

[67] K Simonyan and A Zisserman. Very deep convolutional networks for large-scale image recognition. In *3rd International Conference on Learning Representations (ICLR 2015)*. Computational and Biological Learning Society, 2015.

[68] Yutong Song and Yong Deng. Divergence measure of belief function and its application in data fusion. *IEEE Access*, 7:107465–107472, 2019.

[69] Hélène Soubaras. Towards an axiomatization for the generalization of the kullback-leibler divergence to belief functions. In *Proceedings of the 7th conference of the European Society for Fuzzy Logic and Technology*, pages 1090–1097. Atlantis Press, 2011.

[70] Holger Trittenbach, Adrian Englhardt, and Klemens Böhm. An overview and a benchmark of active learning for outlier detection with one-class classifiers. *Expert Systems with Applications*, 168:114372, 2021.

[71] Dennis Thomas Ulmer, Christian Hardmeier, and Jes Frellsen. Prior and posterior networks: A survey on evidential deep learning methods for uncertainty estimation. *Transactions on Machine Learning Research*, 2023.

[72] Manuel A Vega and Michael D Todd. A variational bayesian neural network for structural health monitoring and cost-informed decision-making in miter gates. *Structural Health Monitoring*, 21(1):4–18, 2022.

[73] Pauli Virtanen, Ralf Gommers, Travis E. Oliphant, Matt Haberland, Tyler Reddy, David Cournapeau, Evgeni Burovski, Pearu Peterson, Warren Weckesser, Jonathan Bright, Stéfan J. van der Walt, Matthew Brett, Joshua Wilson, K. Jarrod Millman, Nikolay Mayorov, Andrew R. J. Nelson, Eric Jones, Robert Kern, Eric Larson, C J Carey, İlhan Polat, Yu Feng, Eric W. Moore, Jake VanderPlas, Denis Laxalde, Josef Perktold, Robert Cimrman, Ian Henriksen, E. A. Quintero, Charles R. Harris, Anne M. Archibald, Antônio H. Ribeiro, Fabian Pedregosa, Paul van Mulbregt, and SciPy 1.0 Contributors. SciPy 1.0: Fundamental Algorithms for Scientific Computing in Python. *Nature Methods*, 17:261–272, 2020.

[74] Frans Voorbraak. A computationally efficient approximation of dempster-shafer theory. *International Journal of Man-Machine Studies*, 30(5):525–536, 1989.

[75] Kaizheng Wang, Keivan Shariatmadar, Shireen Kudukkil Manchingal, Fabio Cuzzolin, David Moens, and Hans Hallez. Creinns: Credal-set interval neural networks for uncertainty estimation in classification tasks. *arXiv preprint arXiv:2401.05043*, 2024.

[76] Yeming Wen, Paul Vicol, Jimmy Ba, Dustin Tran, and Roger Grosse. Flipout: Efficient pseudo-independent weight perturbations on mini-batches. *arXiv preprint arXiv:1803.04386*, 2018.

[77] Bichen Wu, Chenfeng Xu, Xiaoliang Dai, Alvin Wan, Peizhao Zhang, Zhicheng Yan, Masayoshi Tomizuka, Joseph Gonzalez, Kurt Keutzer, and Peter Vajda. Visual transformers: Token-based image representation and processing for computer vision. *arXiv preprint arXiv:2006.03677*, 2020.

[78] Marco Zaffalon. The naive credal classifier. *Journal of statistical planning and inference*, 105(1):5–21, 2002.

[79] Hao Zheng, Zhanlei Yang, Wenju Liu, Jizhong Liang, and Yanpeng Li. Improving deep neural networks using softplus units. In *2015 International Joint Conference on Neural Networks (IJCNN)*, pages 1–4, 2015.

A Mathematical Proof

Toy Problem for Unavailability of Traditional SoftMax The traditional SoftMax activation function cannot be used to define the credal set, as it cannot ensure the condition in Eq. (2) when computing $[\boldsymbol{q}_L, \boldsymbol{q}_U]$ as $\boldsymbol{q}_L = \mathrm{SoftMax}(\boldsymbol{a}_L)$ and $\boldsymbol{q}_U = \mathrm{SoftMax}(\boldsymbol{a}_U)$, respectively.

For example, assuming that we have $\boldsymbol{a}_L := (-1, 0, 1)$ and $\boldsymbol{a}_U := (0, 1, 3)$ from CreNet, the $\boldsymbol{q}_L$ and $\boldsymbol{q}_U$ computed using SoftMax are:

$$\boldsymbol{q}_L = \mathrm{SoftMax}(\boldsymbol{a}_L) = (0.0900, 0.2447, 0.6653),\ \boldsymbol{q}_U = \mathrm{SoftMax}(\boldsymbol{a}_U) = (0.0420, 0.1142, 0.8438).$$

The resulting 'probability intervals' are not properly defined and appear unreasonable, as some lower bounds are considerably higher than the upper bounds.

Mathematical Proof for Interval SoftMax The proof that Interval SoftMax in Eq. (4) does satisfy the conditions in Eq. (2) is straightforward:

$$\begin{aligned}\sum_{i=1}^{C} q_{L_i} &= \sum_{i=1}^{C} \frac{\exp(a_{L_i})}{\sum_{k\neq i}^{C}\exp(\frac{a_{U_k}+a_{L_k}}{2}) + \exp(a_{L_i})} \leq \sum_{i=1}^{C} \frac{\exp(\frac{a_{U_i}+a_{L_i}}{2})}{\sum_{k\neq i}^{C}\exp(\frac{a_{U_k}+a_{L_k}}{2}) + \exp(\frac{a_{U_i}+a_{L_i}}{2})} \\ &= 1 \leq \sum_{i=1}^{C} \frac{\exp(a_{U_i})}{\sum_{k\neq i}^{C}\exp(\frac{a_{U_k}+a_{L_k}}{2}) + \exp(a_{U_i})} = \sum_{i=1}^{C} q_{U_i}\end{aligned}. \tag{16}$$

B Additional Experiments

In this section, Appendix §B.1 discusses the implementation and performance of EU quantification of CreDEs using another uncertainty measure for credal sets: the generalized Hartley measure. Appendix §B.2 performs an ablation study on the value of the hyperparameter K of the PIDR Algorithm 2. Appendix §B.3 assessed CreDEs' performance in the OOD detection task when quantifying uncertainty using TU instead of EU. Appendices §B.4, §B.5, and §B.6 compare CreDEs versus traditional DEs that also apply the DRO strategy, DEs that apply the 'product of experts' ensemble setting [32], and several BNN baselines, respectively. Appendix §B.7 assessed CreDEs in an active learning case study.

B.1 Generalized Hartley Measure for EU Quantification of CreDEs

Uncertainty quantification in credal sets merits further investigation. For instance, recent research [35] has explored, e.g., the use of probability interval length as a measure of epistemic uncertainty, in the special case of binary classification. However, these measures cannot be readily extended to multi-class cases. Recently, the most established methods for decomposing the total uncertainty of credal sets are generalized Entropy [3, 36] and the generalized Hartley Measure [4, 36].

Definition The generalized Hartley measure [4], $\mathrm{GH}(\mathbb{Q})$, measures the non-specificity across the distributions in the credal set, and can be seen as a proxy for its volume [36]. Mathematically, $\mathrm{GH}(\mathbb{Q})$ calculates the expectation of the Hartley measure [26] over all possible subsets $\mathbb{B}$ on the target space $\mathbb{Y}$,[2] as follows [4]:

$$\mathrm{GH}(\mathbb{Q}) = \textstyle\sum_{\mathbb{B}\subseteq\mathbb{Y}} \mathrm{m}_{\mathbb{Q}}(\mathbb{B}) \cdot \log_2(|\mathbb{B}|), \tag{17}$$

in which $\mathrm{m}_{\mathbb{Q}}$ denotes the mass assignment function associated to $\mathbb{Q}$ and $|\mathbb{B}|$ indicates the cardinality of $\mathbb{B}$. $\mathrm{m}_{\mathbb{Q}}(\mathbb{B})$ can be computed using the Möbius inverse of the capacity function $\nu_{\mathbb{Q}}$ [36], as follows:

$$\mathrm{m}_{\mathbb{Q}}(\mathbb{B}) = \textstyle\sum_{\mathbb{A}\subseteq\mathbb{B}} (-1)^{|\mathbb{B}\setminus\mathbb{A}|} \nu_{\mathbb{Q}}(\mathbb{A}), \tag{18}$$

where $\mathbb{B}\setminus\mathbb{A} = \{y | y \in \mathbb{B} \text{ and } y \notin \mathbb{A}\}$ and $\nu_{\mathbb{Q}}$ describes the lower probability of all possible subsets $\mathbb{A} \subseteq \mathbb{B}$.

Efficient Implementation in CreDEs One of the reasons that hinder the application of the Generalized Hartley Measure is its computational complexity. In our work, we proposed an efficient implementation and an approximate approach (the PIDR Algorithm 2) for computing it.

[2] In classification, target space $\mathbb{Y}$ comprises a finite set of class labels, namely $\mathbb{Y} = \{y_1, ..., y_C\}$.

In our case, the lower probability $\nu_{\mathbb{Q}}(\mathbb{A})$ associated with the predicted credal set can be readily computed as follows:

$$\nu_{\mathbb{Q}}(\mathbb{A}) = \max\left(\sum_{y_j \in \mathbb{A}} q^*_{L_j}, 1 - \sum_{y_j \notin \mathbb{A}} q^*_{U_j}\right), \tag{19}$$

where q^*_L and q^*_U are the reachable lower and upper probability values per class in the defined credal set. They can be easily obtained from Eq. (12). Figure 3 illustrates how the lower and upper probabilities q_{L_i}, q_{U_i} that determine the credal set $\mathbb{Q}$ may differ from the probabilities $q^*_{L_i}$ and $q^*_{U_i}$ *actually reachable* for each class within $\mathbb{Q}$.

The full $\mathrm{GH}(\mathbb{Q})$ calculation process is presented in Algorithm 3.

Algorithm 3 $\mathrm{GH}(\mathbb{Q})$ Calculation

Input: $[\boldsymbol{q}^*_L, \boldsymbol{q}^*_U] := \{[q^*_{L_i}, q^*_{U_i}]\}_{i=1}^{C}$; Target space $\mathbb{Y}$
Output: $\mathrm{GH}(\mathbb{Q})$
Initialize: $\mathrm{GH}(\mathbb{Q}) = 0$
for all $\mathbb{B} \subseteq \mathbb{Y}$ **and** $|\mathbb{B}| \geq 2$ **do**
  Initialize: $\mathrm{m}_{\mathbb{Q}}(\mathbb{B}) = 0$
  for all $\mathbb{A} \subseteq \mathbb{B}$ **do**
    Compute $\nu_{\mathbb{Q}}(\mathbb{A})$ using Eq. (19)
    $\mathrm{m}_{\mathbb{Q}}(\mathbb{B}) = \mathrm{m}_{\mathbb{Q}}(\mathbb{B}) + (-1)^{|\mathbb{B}\setminus\mathbb{A}|} \cdot \nu_{\mathbb{Q}}(\mathbb{A})$ (Eq. (18))
  end for
  $\mathrm{GH}(\mathbb{Q}) = \mathrm{GH}(\mathbb{Q}) + \mathrm{m}_{\mathbb{Q}} \cdot \log_2(|\mathbb{B}|)$ (Eq. (17))
end for

Although the use of probability intervals simplifies the calculation of $\mathrm{GH}(\mathbb{Q})$ in general, a significant challenge arises for large values of C (e.g. $C = 100$) due to the complexity of involving subsets of C.

However, when applying our proposed PIDR Algorithm 2, the dimension of the probability interval is reduced from C to K; therefore, calculating $\mathrm{GH}(\mathbb{Q})$ requires only 2^K subsets.

Experimental Validation of GH($\mathbb{Q}$) for OOD Detection The OOD detection results for CreDEs-5 using $\mathrm{GH}(\mathbb{Q})$ are shown in Tables 7, 8 and in Figure 9. Probability Interval Dimension Reduction (PIDR) (Algorithm 2) is utilized with settings $K = 4$ and $K = 10$ when computing $\mathrm{GH}(\mathbb{Q})$ for dataset pairs containing CIFAR10 and CIFAR100/ImageNet, respectively. The results verify that

- Our CreDEs consistently enhance the quality of EU quantification, exhibiting robustness across different uncertainty measures, i.e., the generalized Shannon entropy and the generalized Hartley measure. This improved EU quantification leads to better OOD detection performance compared to Deep Ensemble baselines.
- The proposed PIDR algorithm ensures an efficient implementation of the generalized Hartley measure in our framework. An ablation study on PIDR's hyperparameter is conducted in Appendix §B.2.

Note, however, that applying $K = 10$ for the setting ImageNet vs ImageNet-O does not yield a better result, due to the coarseness of approximating 1000 classes using only 10. This suggests that computing $\mathrm{GH}(\mathbb{Q})$ is still challenging for tasks involving 1000 or more classes.

B.2 Ablation Study on Hyperparameter of PIDR Algorithm

Effect on GH($\mathbb{Q}$) Quantification Figure 10 illustrates the influence of various settings of K on $\mathrm{GH}(\mathbb{Q})$ quantification. The average value $\mathrm{GH}(\mathbb{Q})$ suggests that the use of the PIDR Algorithm 2) results in an underestimated $\mathrm{GH}(\mathbb{Q})$ value, compared to the result without using PIDR ($K = 10$). Consequently, increasing the value of K enhances OOD detection performance. However, as K grows execution time increases exponentially, due to the iterative calculations of $\mathrm{m}_{\mathbb{Q}}(\mathbb{B})$ and $\nu_{\mathbb{Q}}(\mathbb{A})$ in Algorithm 3 across 2^K subsets. The time cost is measured on a single Intel Xeon Gold 8358 CPU@2.6 GHz. While higher than the time cost for EU calculation of DEs ($4.1e^{-4}$ ms), this figure shows that calculating GH for 10 classes ($K = 10$ for 17 ms) remains practical without actual computational constraints. Besides, the numbers reported are for GH calculation without any optimization: a more

Table 7: OOD detection AUROC and AUPRC performance (%, ↑) between CreDEs-5 and DEs-5 based on ResNet50 using EU as uncertainty metrics on CIFAR10/100 vs. SVHN/Tiny-ImageNet and ImageNet vs. ImageNet-O. Results are averaged over 15 runs. Best results are in bold.

ID Samples		CIFAR10				CIFAR100				ImageNet	
OOD Samples		SVHN		Tiny-ImageNet		SVHN		Tiny-ImageNet		ImageNet-O	
Performance Indicator		AUROC	AUPRC	AUROC	AUPRC	AUROC	AUPRC	AUROC	AUPRC	AUROC	AUPRC
DEs-5	$H(\tilde{\boldsymbol{q}})-\tilde{H}(\boldsymbol{q})$	89.58±0.93	92.29±1.00	86.87±0.20	83.02±0.16	73.83±1.97	84.96±1.25	78.80±0.20	74.68±0.27	65.03±0.53	62.77±0.38
CreDEs-5 (ours)	$\overline{H}(\mathbb{Q})-\underline{H}(\mathbb{Q})$	**96.55±0.25**	**98.17±0.17**	**88.10±0.26**	**87.85±0.35**	**78.55±1.15**	**86.57±0.65**	**82.54±0.26**	**77.60±0.44**	**67.82±0.06**	**62.80±0.12**
	$\mathrm{GH}(\mathbb{Q})$	**96.72±0.24**	**98.25±0.17**	**89.54±0.16**	**88.74±0.24**	**79.23±1.19**	**87.17±0.66**	**83.01±0.24**	**78.95±0.44**	63.46±0.06	58.13±0.10

Table 8: AUROC and AUPRC scores (%, ↑) for OOD detection on CIFAR10 vs SVHN/Tiny-ImageNet. Results averaged over 15 runs. The Best results are in bold.

			CIFAR10 vs SVHN		CIFAR10 vs Tiny-ImageNet	
			AUROC	AUPRC	AUROC	AUPRC
VGG16	DEs-5	$H(\tilde{\boldsymbol{q}})-\tilde{H}(\boldsymbol{q})$	82.19±0.82	87.52±0.81	78.58±0.15	73.28±0.23
	CreDEs-5 (Ours)	$\overline{H}(\mathbb{Q})-\underline{H}(\mathbb{Q})$	**87.68±0.73**	**93.47±0.57**	**82.56±0.28**	**80.81±0.52**
		$\mathrm{GH}(\mathbb{Q})$	**86.99±0.72**	**93.18±0.41**	**82.23±0.18**	**80.83±0.24**
ViT Base	DEs-5	$H(\tilde{\boldsymbol{q}})-\tilde{H}(\boldsymbol{q})$	77.71±1.67	88.73±0.32	82.27±0.79	78.85±0.81
	CreDEs-5 (Ours)	$\overline{H}(\mathbb{Q})-\underline{H}(\mathbb{Q})$	**88.57±2.08**	**93.24±1.25**	**88.73±0.32**	**87.84±0.52**
		$\mathrm{GH}(\mathbb{Q})$	**89.07±1.66**	**93.32±1.06**	**89.19±0.42**	**88.21±0.58**

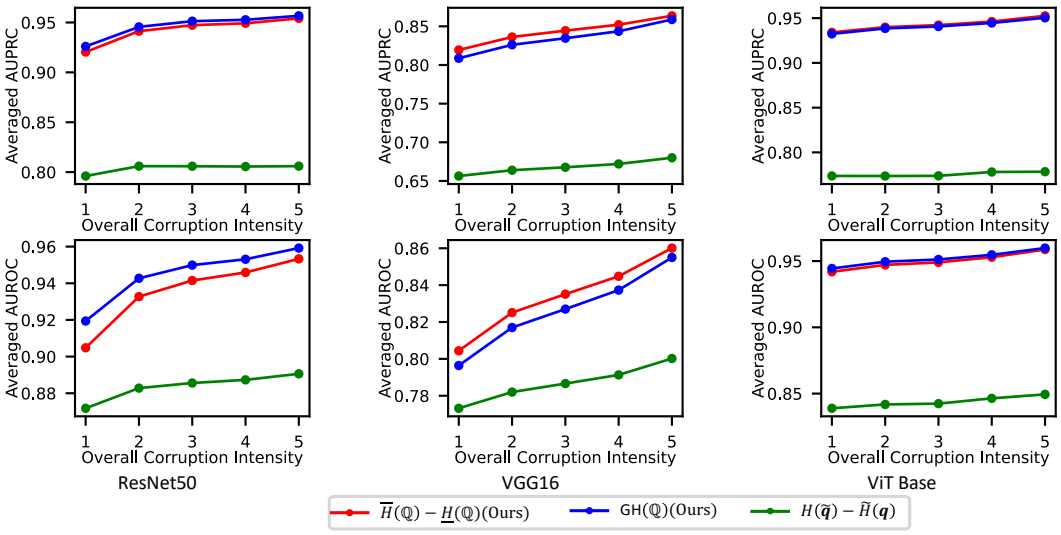

Figure 9: OOD detection on CIFAR10 vs CIFAR10-C against increased corruption intensity, using ResNet50, VGG16, and ViT Base as backbones.

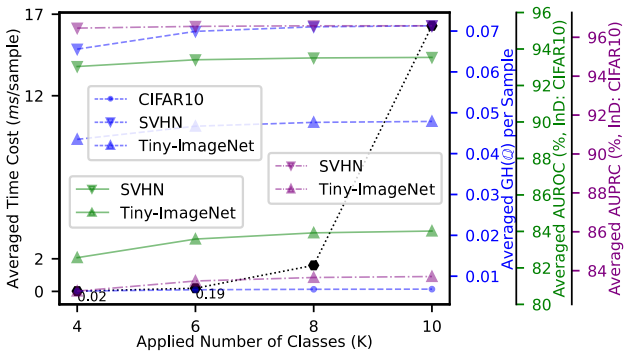

Figure 10: Average time cost of $\mathrm{GH}(\mathbb{Q})$ (black dotted line) and $\mathrm{GH}(\mathbb{Q})$ value per sample across various datasets (blue lines), along with the AUROC/AUPRC scores (green/purple lines) for OOD detection versus increasing values of K.

efficient code implementation could significantly reduce the cost. The effect of various settings of K on $\overline{H}(\mathbb{Q})$ is shown as follows.

Effect on TU Quantification In this experiment, we examine the effect of K on TU estimation. Figure 11 shows the average values of TU estimates ($\overline{H}(\mathbb{Q})$) sample, together with the AUROC and AUPRC scores for CIFAR100 vs. SVHN/Tiny-ImageNet. The results indicate that applying PIDR (Algorithm 2) tends to underestimate TU values. Consequently, increasing the value of K improves the OOD detection performance, but it also leads to an increase in execution time. This is because solving the constrained optimization problem in Eq. (13) involves more variables and constraints.

The reported time cost is measured on a single Intel Xeon Gold 8358 CPU@2.6 GHz, without optimization in the calculation process. We believe a more efficient code implementation could significantly mitigate this.

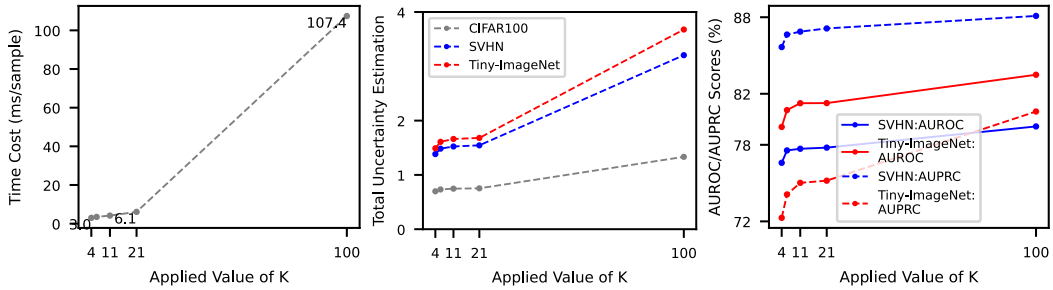

Figure 11: Average$\overline{H}(\mathbb{Q})$ time cost, average $\overline{H}(\mathbb{Q})$ value per sample, and OOD performance on the OOD detection benchmark (CIFAR100 vs. SVHN/Tiny-ImageNet) for increasing values of K.

B.3 Total Uncertainty Estimation Evaluation via OOD Detection

In further additional experiments, we also assess the quality of the *total uncertainty* (TU) estimates produced by CreDEs-5 on the various OOD detection benchmarks [43, 54]. The results in Tables 9 and 10 consistently demonstrate CreDEs' improved OOD detection performance using TU as a metric.

B.4 Comparison between CreDEs and DEs with DRO Strategy

In this experiment, we additionally train 15 ResNet50-based SNNs on the CIFAR10 and CIFAR100 datasets using the DRO loss component and the same training strategy as in Algorithm 1, respectively. For a fair comparison, we set $\delta = 0.5$ (just as for CreNets), using the same random seeds and training epochs. Other training configurations are described in Appendix §C. We named the resulting deep ensembles with 5 ensemble members as DEs*-5.

Table 9: OOD detection AUROC and AUPRC performance (%, ↑) between CreDEs-5 and DEs-5 based on ResNet50 using TU as uncertainty metrics on CIFAR10/100 vs. SVHN/Tiny-ImageNet and ImageNet vs. ImageNet-O. Results are averaged over 15 runs. Best results in bold.

ID Samples		CIFAR10				CIFAR100				ImageNet	
OOD Samples		SVHN		Tiny-ImageNet		SVHN		Tiny-ImageNet		ImageNet-O	
Performance Indicator		AUROC	AUPRC	AUROC	AUPRC	AUROC	AUPRC	AUROC	AUPRC	AUROC	AUPRC
DEs-5	$H(\tilde{\boldsymbol{q}})$	94.80±0.43	97.26±0.29	88.80±0.19	87.21±0.29	78.53±1.94	**88.83±1.01**	80.75±0.15	77.65±0.19	50.20±0.07	50.43±0.06
CreDEs-5	$\overline{H}(\mathbb{Q})$	**95.71±0.42**	**97.73±0.27**	**89.02±0.10**	**88.02±0.15**	**79.44±1.45**	88.10±0.79	**83.49±0.17**	**80.61±0.33**	**67.56±0.06**	**62.79±0.18**

Table 10: OOD detection AUROC and AUPRC performance (%, ↑) between CreDEs-5 and DEs-5 based on VGG16 and ViT Base using TU as uncertainty metrics on CIFAR10 vs. SVHN/Tiny-ImageNet. Results are averaged over 15 runs. Best results in bold.

		VGG16				ViT Base			
		SVHN (OOD)		Tiny-ImageNet (OOD)		SVHN (OOD)		Tiny-ImageNet (OOD)	
		AUROC	AUPRC	AUROC	AUPRC	AUROC	AUPRC	AUROC	AUPRC
DEs-5	$H(\tilde{\boldsymbol{q}})$	84.50±0.49	90.78±0.35	79.40±0.10	75.91±0.14	79.80±1.75	87.97±1.17	83.81±0.81	81.68±0.89
CreDEs-5	$\overline{H}(\mathbb{Q})$	**87.05±0.80**	**93.36±0.42**	**82.14±0.14**	**80.81±0.16**	**87.30±1.77**	**92.24±1.15**	**88.17±0.44**	**86.94±0.60**

We compare test accuracy and ECE for DEs*-5 and CreDEs-5 in Table 11, and their OOD detection performance on the CIFAR10/100 (ID) vs SVHN/Tiny-ImageNet (OOD) benchmark in Table 12.

Table 11: Test accuracy and ECE of DEs*-5 and CreDEs-5 on the CIFAR10 and CIFAR100 datasets. Best results in bold.

		CIFAR10		CIFAR100	
		Test Accuracy	ECE	Test Accuracy	ECE
DEs*-5		91.53±0.22	0.0159±0.0019	68.34±0.52	0.0372±0.0033
CreDEs-5	$\hat{\imath}_{\min}$	**93.75±0.11**	**0.0092±0.0016**	**79.54±0.21**	**0.0366±0.0025**
	$\hat{\imath}_{\max}$	**93.74±0.11**	**0.0108±0.0017**	**79.65±0.19**	**0.0268±0.0023**

Table 12: OOD detection performance comparison of DEs*-5 and CreDEs-5 using the dataset pairs CIFAR10/100 (ID) vs SVHN/Tiny-ImageNet (OOD).

		CIFAR10 (ID)				CIFAR100 (ID)			
		SVHN (OOD)		Tiny-ImageNet (OOD)		SVHN (OOD)		Tiny-ImageNet (OOD)	
		AUROC	AUPRC	AUROC	AUPRC	AUROC	AUPRC	AUROC	AUPRC
TU	DEs*-5:$H(\tilde{\boldsymbol{q}})$	91.82±0.96	95.13±0.70	86.26±0.30	84.09±0.42	78.70±1.61	**88.20±0.91**	76.99±0.28	73.03±0.37
	CreDEs-5:$\overline{H}(\mathbb{Q})$	**95.71±0.42**	**97.73±0.27**	**89.02±0.10**	**88.02±0.15**	**79.44±1.45**	88.10±0.17	**83.49±0.17**	**80.61±0.33**
EU	DEs*-5:$H(\tilde{\boldsymbol{q}})$−$\tilde{H}(\boldsymbol{q})$	87.21±1.49	91.09±1.39	84.58±0.30	80.80±0.42	74.38±1.39	84.67±0.86	75.27±0.38	70.80±0.48
	CreDEs-5:$\overline{H}(\mathbb{Q})$−$\underline{H}(\mathbb{Q})$	**96.55±0.25**	**98.17±0.17**	**88.10±0.26**	**87.85±0.35**	**78.55±1.15**	**86.57±0.65**	**82.54±0.26**	**77.60±0.44**
	CreDEs-5:GH($\mathbb{Q}$)	**96.72±0.24**	**98.25±0.17**	**89.54±0.16**	**88.74±0.24**	**79.23±1.19**	**87.17±0.66**	**83.01±0.24**	**78.95±0.44**

The reported results demonstrate that CreDEs-5 outperforms DEs*-5 ensembles by achieving higher test accuracy and lower ECE values. Concerning OOD detection tasks, it can be found that CreDEs in general improve the AUPRC and AUROC scores using either the TU or the EU metric, pretty much across the board. These results suggest that CreDEs provide higher-quality EU and TU estimation.

In Table 12, a 0.1% drop in AUPRC using the TU metric can be observed. However, remember that CreDEs calculate TU (using the upper entropy) by solving a constrained optimization problem in Eq. (13) using a numerical solver from SciPy. The slight performance decrease is likely due to numerical errors during the optimization process.

B.5 Comparison between CreDEs and DEs with POE Ensemble Setting

In this experiment, we conduct a comparison between our CreDEs and DEs with the 'product of experts' (POE) [32] ensemble setting, as opposed to the more commonly employed 'mixture of

experts' approach in our primary analysis. Here, DEs^p-5 denotes the deep ensembles that process the final predictions from the ensemble members using the POE strategy. The experimental setup mirrors that used by OOD detection benchmarks, involving data pairs CIFAR10 (ID) vs SVHN/Tiny-ImageNet (OOD).

Table 13 shows that DEs^p-5 could improve test accuracy but significantly reduce the calibration performance of DEs-5 (larger ECE values). Among these comparisons, CreDEs-5 emerged as the most superior method. Furthermore, we evaluate the uncertainty estimation through the OOD detection benchmark. Specifically, =the entropy of the final prediction of DEs^p-5 is calculated to quantify the total uncertainty. For CreDEs-5 and DEs-5, we use the upper entropy, $\overline{H}(\mathbb{Q})$, and $H(\tilde{\boldsymbol{q}})$, respectively. The results in Table 14 consistently demonstrate the superior performance of our method. Although the POE strategy improves the test accuracy of classical DEs, it significantly degrades calibration performance and leads to inferior OOD detection performance.

Table 13: Test accuracy (ACC) (%) and ECE comparison on the CIFAR10 dataset, using the ResNet50, VGG16, and ViT Base architectures.

	ResNet50		VGG16		ViT Base	
	ACC	ECE	ACC	ECE	ACC	ECE
CreDEs-5 ($\hat{i}_{\max}$)	**93.74±0.11**	**0.0109±0.0017**	**87.92±0.11**	**0.0611±0.0012**	**93.59±0.39**	**0.0104±0.0012**
CreDEs-5 ($\hat{i}_{\min}$)	**93.75±0.11**	**0.0092±0.0016**	**87.94±0.11**	**0.0203±0.0014**	**93.60±0.40**	**0.0107±0.0014**
DEs-5	93.32±0.13	0.0131±0.0010	85.53±0.10	0.0815±0.0011	90.43±0.97	0.0181±0.0019
DEs^p-5	93.47±0.11	0.0610±0.0011	85.55±0.08	0.1368±0.0008	90.56±0.90	0.0894±0.0087

Table 14: OOD detection performance comparison (%) on CIFAR10 vs SVHN/Tiny-ImageNet, using the ResNet50, VGG16, and ViT Base architectures.

	ResNet50				VGG16				ViT Base			
	SVHN		Tiny-ImageNet		SVHN		Tiny-ImageNet		SVHN		Tiny-ImageNet	
	AUROC	AUPRC	AUROC	AUPRC	AUROC	AUPRC	AUROC	AUPRC	AUROC	AUPRC	AUROC	AUPRC
CreDEs-5	**95.71±0.42**	**97.73±0.27**	**89.02±0.10**	**88.02±0.15**	**87.05±0.80**	**93.36±0.42**	**82.14±0.14**	**80.81±0.16**	**87.30±1.77**	**92.24±1.15**	**88.17±0.44**	**86.94±0.60**
DEs-5	94.80±0.43	97.26±0.29	88.80±0.19	87.21±0.29	84.50±0.49	90.78±0.35	79.40±0.10	75.91±0.14	79.80±1.75	87.97±1.17	83.81±0.81	81.67±0.89
DEs^p-5	93.90±0.24	96.10±0.21	88.03±0.20	84.11±0.32	84.10±0.22	89.83±0.16	78.11±0.08	72.23±0.16	82.41±1.56	88.51±0.95	83.21±1.02	78.24±1.17

B.6 Comparison between CreDEs and Bayesian Neural Networks

As discussed in the main body, the main reason for excluding Bayesian neural network (BNN) approaches in our main evaluation is that they generally have difficulty scaling to large datasets and complex network architectures [54]. In this section, we conducted an additional comparison between CreDEs and DEs, MCDropout [22], and two TensorFlow-standardized BNNs (BNN-R [51] and BNN-F [76]). All the models are trained on the ResNet50 for the CIFAR10 dataset from scratch. The input data shape is (32, 32, 3). The Adam optimizer is applied with a learning rate scheduler, initialized at 0.001. The learning rate is subject to a reduction of 0.1 at epochs 80 and 120. For BNNs, 10 forward passes are used for uncertainty estimation.

The uncertainty evaluation via OOD detection on the CIFAR10 vs SVHN/Tiny-ImageNet dataset is reported in Table 15. The results consistently demonstrate the significant improvements of our CreDEs.

B.7 Case Study on Active Learning Settings

Active learning (AL) aims to efficiently train models with minimal data by acquiring additional samples from a vast pool of unlabeled data, which are then labeled by experts [11]. After each acquisition step, the model is retrained using the expanded training set. The iterative process continues until either the desired accuracy or the maximum allowable acquired samples are reached. Efficient data acquisition can be a reliable estimate of the uncertainty of models [23, 54].

Setup We deploy CreDEs-5 ($\delta = 0.5$) and DEs-5 (baseline) using the ResNet18 architecture and utilizing clean MNIST samples in the pool set. TU and EU estimations from each approach for the acquisition functions are utilized. We begin with an initial training set of 20 randomly selected MNIST points.

Table 15: OOD detection AUROC and AUPRC performance (%, ↑) between CreDEs-5 and Bayesian models based on ResNet50 using EU and TU as uncertainty metrics on CIFAR10 vs. SVHN/Tiny-ImageNet. Results are averaged over 15 runs. The best results are in bold. The 'drop' denotes the dropout rate applied to MCDropout.

Model		Epistemic Uncertainty Measure as Metric				Total Uncertainty Measure as Metric			
		SVHN (OOD)		Tiny-ImageNet (OOD)		SVHN (OOD)		Tiny-ImageNet (OOD)	
		AUROC	AUPRC	AUROC	AUPRC	AUROC	AUPRC	AUROC	AUPRC
CreDEs-5		**79.14±1.49**	**86.84±1.18**	**82.85±0.29**	**80.71±0.42**	**81.00±0.75**	**88.66±0.46**	**84.06±0.11**	**82.16±0.13**
DEs-5		73.53±1.65	83.81±1.42	76.13±0.58	70.86±0.67	77.93±0.65	84.92±0.39	80.22±0.26	76.94±0.30
BNN-R		70.30±3.55	82.41±2.45	72.91±2.01	67.82±2.10	73.37±2.00	82.69±1.58	73.98±1.85	70.52±1.89
BNN-F		70.15±4.38	82.04±3.01	73.66±1.46	68.52±1.53	73.77±2.62	82.90±1.71	74.57±1.30	71.11±1.29
MCDropout	0.1 drop	74.19±1.55	82.93±1.01	75.04±0.77	68.25±1.31	76.92±1.85	85.93±1.22	77.48±0.56	73.63±0.62
	0.4 drop	61.66±1.89	73.47±1.27	67.24±1.36	59.55±1.41	79.25±0.96	86.04±0.77	76.04±0.57	72.73±0.65

In each iteration, we acquire the 5 samples with the highest reported uncertainty estimates (EU or TU per model). After each step, we train models using the Adam optimizer for 20 epochs and select the one with the best accuracy from the validation set. AL process stops when the training set size reaches 150.

Results Figure 12 shows the result comparison between CreDEs-5 and DEs-5 using TU and EU estimates as the acquisition functions per model. In the evaluation using MNIST, aiming for a 90% accuracy or a maximum sample count of 150, CreDEs-5 employing acquisition functions TU ($\overline{H}(\mathbb{Q})$) and EU (GH($\mathbb{Q}$)), demonstrates superior performance compared to DEs-5 using TU ($H(\tilde{\boldsymbol{q}})$). In addition, CreDEs-5 with EU ($\overline{H}(\mathbb{Q}) - \underline{H}(\mathbb{Q})$) outperforms DEs-5 with EU ($H(\tilde{\boldsymbol{q}}) - \tilde{H}(\boldsymbol{q})$). The additional evidence verifies the improved quality of EU and TU estimation of CreDEs, compared to DEs. In future work, we aim to explore the potential integration of our methods into other active learning benchmarks [70] and real-world applications or further improve on them.

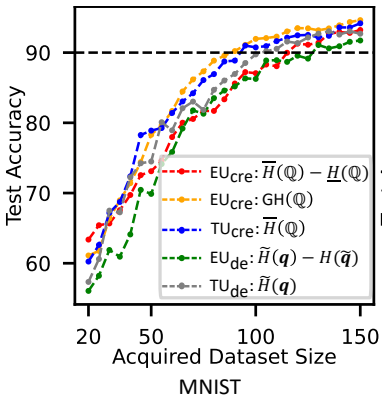

Figure 12: AL experiments using different acquisition functions. Achieved test accuracy vs. acquired training set size.

C Experiment Implementation Details

For the main experiments on the ResNet50 backbone, we used two Tesla P100-SXM2-16GB GPUs as devices to independently train 15 SNNs and CreNets using CIFAR10 and CIFAR100 datasets. The input shape of both networks was (224, 224, 3). We employed the Adam optimizer, with a learning rate scheduler set at 0.001 and reduced to 0.0001 during the last five training epochs.

Figure 13 shows the averaged training and validation accuracy for training process monitoring.

In the ImageNet experiments, we employed three NVIDIA A100-SXM4-80GB GPUs. To create deep ensembles, we independently retrained 15 deep SNNs based on a pre-trained ResNet50 model for 3 epochs, using the Adam optimizer with an initialized learning rate of $1e^{-6}$. For CreDEs, we initialized CreNet weights using a pre-trained ResNet50 model and independently retrained 15 CreNet models for 5 epochs, using the Adam optimizer with an initialized learning rate of $1e^{-5}$. The choice of a larger learning rate value and epoch count for CreNets is a consequence of their modified final later compared to SNNs. For the ablation study on various network architectures, we again utilized two Tesla P100-SXM2-16GB GPUs and one NVIDIA A100-SXM4-80GB GPU as devices to independently train 15 SNNs and CreNets, based on VGG16 and ViT Base architectures, respectively, and using the CIFAR10 dataset. VGG16-based SNNs and CreNets were trained for 20 epochs. SNNs and CreNets using the ViT Base backbone were trained for 25 and 40 epochs, respectively. The input

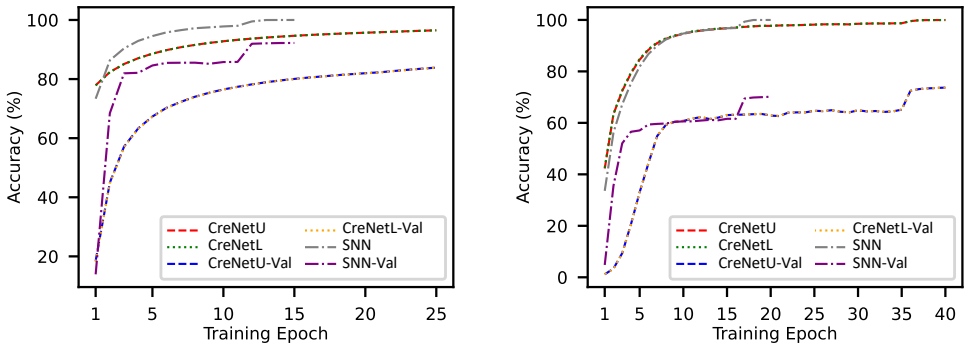

(a) CIFAR10 (b) CIFAR100

Figure 13: Averaged training and validation (Val) accuracy (%) for CreNets and SNNs over 15 runs. The U and L in the labels of CreNets represent accuracies associated with upper and lower probability bounds, namely $\hat{\imath}_{\max}$ and $\hat{\imath}_{\min}$, respectively.

shape for both networks was set to (224, 224, 3). For optimization, we employed the Adam optimizer with a learning rate scheduler initialized at 0.001 and reduced to 0.0001 during the final 5 training epochs.

Training Complexity We did not include the report of training time complexity in the main paper as CreNets use a custom training loop, unlike the TensorFlow-standardized training of standard neural networks (SNNs), precluding a fair comparison.

Nevertheless, we did train a single CreNet and a single SNN based on the ResNet50 architecture on the CIFAR10 dataset, from scratch and on a single A100 GPU. The training time per epoch is 16.36s for the SNN and 73.77s for CreNet, respectively. Given the evidence that CreNets only marginally increases the inference time (single forward pass), we are optimistic that by standardizing and optimizing the customized training loop and adopting a more efficient code implementation of Algorithm 1, we could significantly reduce the training load.

Further Discussion on Inference Complexity As we discussed previously, regarding inference time, doubling the final layer nodes would slightly increase the inference time. For instance, the inference time per sample for a ResNet50 architecture on the ImageNet dataset is 5.5 ms for a single standard neural network, vs 5.7 ms for a single CreNet (a marginal increase). The inference cost on the CIFAR10/100 dataset reported in Table 16 further demonstrates a slight increase in inference complexity in our method. Moreover, Table 17 presents the inference cost, evaluated on a single AMD EPYC 7643 48-core CPU. The results indicate no significant overhead of our CreDEs and also demonstrate that employing VGG16, a lighter model architecture compared to ResNet50, substantially reduces the inference cost for both DEs and CreDEs.

Table 16: Complexity comparison between ResNet50-based SNNs and CreNets using CIFAR10/100 datasets. The inference cost per dataset is measured by a single NVIDIA P100 SXM2-16GB GPU for both models.

Dataset	Model	Parameters (million)	Inference time per sample (ms)
CIFAR10	SNNs vs CreNets	26.216 vs 26.221	60.6±0.7 vs 63.0±1.1
CIFAR100	SNNs vs CreNets	26.262 vs 26.314	62.5±0.5 vs 63.1±0.7

Table 17: Inference cost comparison on CPU between SNNs and CreNets per single CIFAR10 input of different architectures.

	VGG16 (ms)	ResNet50 (ms)
SNNs vs CreNets	19.2±3.8 vs 23.1±5.2	148.2±49.0 vs 163.3±39.4

Regarding the uncertainty estimation cost, we report the cost of calculating the Generalized Hartley (GH) measure and the upper entropy in Figures 10 and 11, respectively. For example, the time cost for GH calculation for CIFAR10 without approximation is 17 ms (0.02 ms in the reduced case considering 4 out of 10 classes) while calculating the EU in deep ensembles for CIFAR10 takes

1×10^{-4}ms, measured on the same single CPU. Though higher CreDEs remain practical without actual computational constraints. In addition, the reported numbers are without code efficiency optimization: a more efficient code implementation could significantly reduce the cost.

The practical takeaway here is that, as demonstrated by extensive experimental variation, our CreDEs exhibit strong potential to enhance the uncertainty quantification performance of DEs in real-world applications, with only a modest increase in computational complexity. However, if DEs are already deemed impractical due to computational limitations, our CreDEs would not be a suitable alternative.

D Discussions on Ensemble Approaches

D.1 Rationale for Averaging Ensemble Strategy

The randomness of parameter initialization in neural networks is one of the reasons leading to (epistemic) uncertainty about the 'ground-truth' model. As we gather more information, both epistemic and total uncertainty should decrease. For example, if we assume that we can train an infinite number of standard neural networks, then the Deep Ensembles would eliminate the source of ignorance caused by the randomness of parameter initialization.

Our proposed averaging approach to creating an ensemble of CreNets follows a similar rationale. Specifically, if we aggregate an infinite number of ensemble members, the uncertainty caused by the randomness would vanish. The outputted probability interval of CreDEs, primarily acknowledges the lack of precise insights into the divergence between the training and test distributions.

D.2 Possible Alternative Ensemble Approaches

CreDEs aggregate predictions from multiple individually trained CreNets, producing credal sets based on probability intervals. In addition to averaging, two alternative approaches, namely union (disjunctive combination) and intersection (conjunctive combination) [17], can be envisaged.

These alternative methods are illustrated in Figure 14.

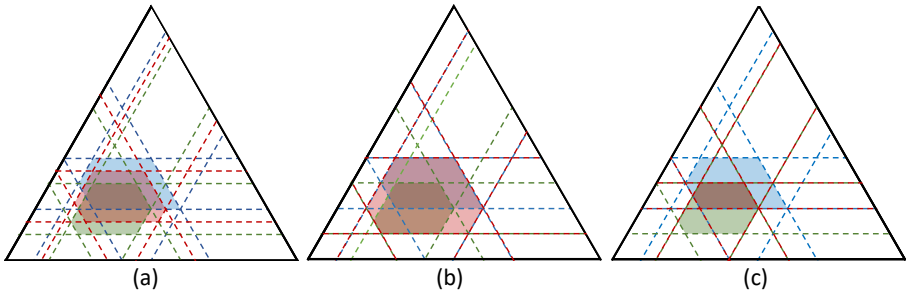

Figure 14: Representation of three ensemble approaches: averaging (a), union (b), and intersection (c). In each subfigure, the ultimate credal set (highlighted in dark red) is formed by aggregating two individual credal sets, each constrained by probability intervals indicated in light green and blue, respectively.

Averaging CreDEs average the upper and lower probabilities per class from M individually-trained CreNets and predict the aggregated probability intervals, denoted as $[\tilde{\boldsymbol{q}}^*_L, \tilde{\boldsymbol{q}}^*_U]$, as discussed in Eq. (14). It can be proved that $[\tilde{\boldsymbol{q}}^*_L, \tilde{\boldsymbol{q}}^*_U]$ is guaranteed to generate a non-empty credal set, as follows:

$$\sum_{i=1}^{C} \tilde{q}^*_{L_i} = \frac{1}{M} \sum_{m=1}^{M} \sum_{i=1}^{C} q^*_{L_{m_i}} \leq 1 \leq \frac{1}{M} \sum_{m=1}^{M} \sum_{i=1}^{C} q^*_{U_{m_i}} = \sum_{i=1}^{C} \tilde{q}^*_{U_i}. \tag{20}$$

The semantic behind averaging is that we equally trust all pieces of information (individual credal sets) without judging the authenticity of the information. Similar to traditional deep ensembles (DEs), the averaging ensemble approach can alleviate the influence of training process randomness.

Union Given a collection of convex probability intervals, denoted as $\{[\boldsymbol{q}^*_{L_m}, \boldsymbol{q}^*_{U_m}]\}_{m=1}^{M}$, De Campos et al. have proposed the computationally efficient way to calculating the union of credal sets [17], as

follows:

$$\tilde{q}^*_{L_i} = \min_{m\in\{1,\ldots,M\}} q^*_{L_{m_i}},\ \tilde{q}^*_{U_i} = \max_{m\in\{1,\ldots,M\}} q^*_{U_{m_i}}. \tag{21}$$

The union ensemble method implies that at least one piece of information is considered to be true. The union operation in Eq. (21) has a significant limitation, as it results in an expanded credal set and introduces an overestimation effect on the precise union of credal sets, as shown in Figure 14.

Intersection A collection of convex probability intervals $\{[\boldsymbol{q}^*_{L_m}, \boldsymbol{q}^*_{U_m}]\}_{m=1}^M$ can formulate an intersection as

$$\tilde{q}^*_{L_i} = \max_{m\in\{1,\ldots,M\}} q^*_{L_{m_i}},\ \tilde{q}^*_{U_i} = \min_{m\in\{1,\ldots,M\}} q^*_{U_{m_i}}. \tag{22}$$

However, the obtained $[\tilde{\boldsymbol{q}}^*_L, \tilde{\boldsymbol{q}}^*_U]$ does not inherently satisfy the condition outlined in Eq. (2) for constructing a credal set [17]. Therefore, the intersection approach is not applicable in CreDEs.

Empirical evaluation In this experiment, we mainly evaluate the impact of averaging and union ensemble approaches on the EU estimation (GH($\mathbb{Q}$)) of CreDEs. Utilizing 15 individually trained ResNet50-based CreNets on CIFAR10 dataset, we formulate 15 CreDEs-M by varying the ensemble number M from 2 to 10 through averaging and union ensemble methodologies. Each kind of CreDEs-M is assessed for the averaged GH($\mathbb{Q}$) concerning samples and the quantity of CreDEs-M, and the averaged standard deviation (STD) of GH($\mathbb{Q}$) related to samples and the quantity of CreDEs-M. The results are plotted in Figure 15 (b) and (a), respectively. Besides, we also present the AUPRC and AUROC scores of OOD detection using GH($\mathbb{Q}$) as the uncertainty metric in Figure 15 (c) and (d), accordingly.

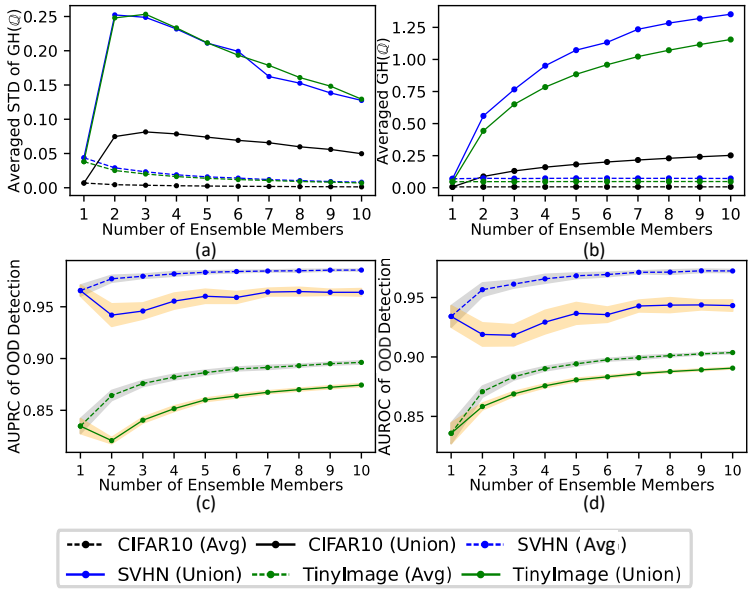

Figure 15: Impact of averaging (Avg) and union on the EU estimation of CreDEs on OOD detection benchmark involving CIFAR10 vs. SVHN/Tiny-ImageNet (TinyImage), implemented on ResNet50 architecture.

Figure 15 (a) illustrates a reduction in the averaged standard deviation (STD) of GH($\mathbb{Q}$) estimates as the number of ensemble members increases. This suggests that averaging the ensemble helps mitigate the uncertainty resulting from the randomness in the CreNet training process. Consequently, the AUROC and AUPRC scores, shown in Figure 15 (c) and (d), exhibit enhancement through the utilization of the averaging ensemble approach, accompanied by a concurrent reduction in the STDs of the scores as the number of ensemble members increases. In contrast, Figure 15 (b) highlights the overestimation of EU across various datasets when employing the union ensemble method. While the average EU estimates for ID samples are overall lower than those for OOD instances, the overestimation may lead to OOD mis-detection in some specific samples. This explains the "fluctuations" in the associated AUPRC and AUROC score curves in Figure 15.

E Further Discussion on Future work

E.1 Generalizing Cross-Entropy for Lower/Upper Probability

As stated in Sec. 2.2.2, calculating the cross-entropy (CE) loss for the lower and upper probability works due to the 'one-hot' labeling nature of the ground truth vector $\boldsymbol{t}$. However, generalizing the CE, which corresponds to the Kulback Leibler (KL) divergence

$$D_{KL}(\boldsymbol{t}|\boldsymbol{q}) = \sum_{j=1,...,C} t(j) \log \left(\frac{t(j)}{q(j)} \right)$$

between a predicted probability vector $\boldsymbol{q}$ and the general ground truth vector $\boldsymbol{t}$, to lower/upper probabilities is still an open research subject [68, 69].

In our case, the credal set $\mathbb{Q}$ is defined by the outputted proper probability intervals $[\boldsymbol{q}_L, \boldsymbol{q}_U]$. Therefore, the KL divergence for a lower probability inducing a credal set may be calculated by:

- Finding the probability vector that best approximates it. For probability intervals, there are two established such ways: normalizing either the lower or the upper probability (see [74]) or computing the so-called 'intersection probability' (see [15]).
- Computing the KL divergence between the ground truth vector and the approximation obtained.

In future work, we aim to investigate the approach and compare those other well-founded methods for calculating the cross-entropy loss with the one used in the paper.

E.2 Theoretical Coverage Guarantees

In the current stage, our CreNets do not provide coverage guarantees, e.g., on how likely it is for the divergence of future data distributions to be within the modeled bounds. Nevertheless, various approaches to incorporating statistical guarantees in our framework can be envisaged.

In particular, a CreDE, being a classifier, can be employed as the 'underlying model' in an inductive *conformal learning* framework [64], which builds an empirical cumulative distribution of the 'non-conformity' scores of a set of calibration samples and at test time outputs the set of labels whose empirical CDF is above a desired significance level ϵ (e.g., 90%).

Namely, given a test input x and the associated predictive system of probability intervals $[q_{L_c}, q_{U_c}], c = 1, ..., C$ (the output of CreDE), a sensible choice, for instance, is to set as non-conformity score of a pair (test input, class), (x, c), the complement of the upper probability for that class, given input x:

$$s(x, c) \doteq 1 - q_{U_c}$$

(i.e., a label c would be considered 'non-conformal' if its predicted upper probability, for that input x, is low), and compute predictive regions as standard in conformal learning:

$$\Gamma(x) = c \in \mathcal{C} : p^c > \epsilon,$$

where

$$p^c = \frac{|(x_j, c_j) : s(x_j, c_j) > s(x, c)|}{q + 1} + u \cdot \frac{|(x_j, c_j) : s(x_j, c_j) = s(x, c)|}{q + 1},$$

(x_j, c_j) is the j-th calibration point, q is the number of calibration points, and $u \sim \mathcal{U}(0, 1)$ (the uniform distribution on the interval $(0, 1)$).

We plan to explore this integration as the next step of our future work.

E.3 Extension for Regression Framework

The vast majority of papers using credal sets in machine learning focus on classification [12, 5, 78], or, more recently, on self-supervised learning (but still in a classification setting [37]). Nevertheless, a recent study [19] has shown that the formalism of belief functions (a special class of credal sets) can

be extended to regression, by leveraging random fuzzy sets. It might thus be possible to explore such connections between probability intervals and random fuzzy sets and devise a suitable regression framework based on CreDEs.

The following section outlines a more direct possible extension of CreDEs to regression problems as a future research direction.

Remember that a CreNet outputs a credal set on the simplex of probability distributions over the classes. Each vertex of this credal set is therefore a probability distribution over the target space (the set of classes C for classification).

On the other hand, a Bayesian regressor network (trained to learn a distribution of its weights) would output a (continuous) probability density over the target space (for the sake of simplicity, assume $Y = \mathbb{R}$).

One could then train an ensemble of Bayesian regressor networks to predict a credal set with a fixed number of vertices (one network outputting one vertex probability) so that the final predicted credal set is the convex closure of those. Figure 16 illustrates the concept briefly.

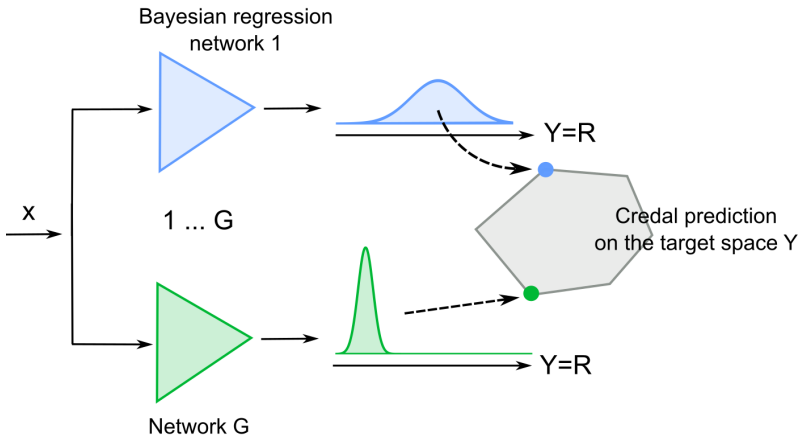

Figure 16: Concept of a credal regressor.

The Distributionally Robust Optimization (DRO) framework employed for CreDE training is to model the divergence between the data distribution of samples belonging to G different groups within the training set. A full DRO formulation with G loss components, in combination with Bayesian deep learning techniques such as variational inference, could then be employed to drive the training of the G credal vertex networks, encouraged to generate diverse (probabilistic) predictions to model different possible data distributions, in a generalization of the two-component loss used here.

Broader Impacts

The main objective of this paper is to advance the field of Machine Learning by improving the quality of uncertainty quantification. There are many potential societal consequences of our work, none of which we feel must be specifically highlighted here. The proposed method demonstrates superior performance in detecting out-of-distribution (OOD) samples. Such capability can potentially safeguard end users from misguided decisions that stem from the incorrect predictions of neural networks on OOD instances. Therefore, our approach can potentially improve the safety, reliability, and trustworthiness of machine learning systems for classification tasks and be applied in mission-critical domains, such as autonomous driving and medical sciences.

NeurIPS Paper Checklist

1. **Claims**

   Question: Do the main claims made in the abstract and introduction accurately reflect the paper's contributions and scope?

   Answer: [Yes]

   Justification: The main claims made in the abstract and introduction accurately reflect our paper's contributions and scope.

   Guidelines:

   - The answer NA means that the abstract and introduction do not include the claims made in the paper.
   - The abstract and/or introduction should clearly state the claims made, including the contributions made in the paper and important assumptions and limitations. A No or NA answer to this question will not be perceived well by the reviewers.
   - The claims made should match theoretical and experimental results, and reflect how much the results can be expected to generalize to other settings.
   - It is fine to include aspirational goals as motivation as long as it is clear that these goals are not attained by the paper.

2. **Limitations**

   Question: Does the paper discuss the limitations of the work performed by the authors?

   Answer: [Yes]

   Justification: We discuss the limitations in the Conclusion Section.

   Guidelines:

   - The answer NA means that the paper has no limitation while the answer No means that the paper has limitations, but those are not discussed in the paper.
   - The authors are encouraged to create a separate "Limitations" section in their paper.
   - The paper should point out any strong assumptions and how robust the results are to violations of these assumptions (e.g., independence assumptions, noiseless settings, model well-specification, asymptotic approximations only holding locally). The authors should reflect on how these assumptions might be violated in practice and what the implications would be.
   - The authors should reflect on the scope of the claims made, e.g., if the approach was only tested on a few datasets or with a few runs. In general, empirical results often depend on implicit assumptions, which should be articulated.
   - The authors should reflect on the factors that influence the performance of the approach. For example, a facial recognition algorithm may perform poorly when image resolution is low or images are taken in low lighting. Or a speech-to-text system might not be used reliably to provide closed captions for online lectures because it fails to handle technical jargon.
   - The authors should discuss the computational efficiency of the proposed algorithms and how they scale with dataset size.
   - If applicable, the authors should discuss possible limitations of their approach to address problems of privacy and fairness.
   - While the authors might fear that complete honesty about limitations might be used by reviewers as grounds for rejection, a worse outcome might be that reviewers discover limitations that aren't acknowledged in the paper. The authors should use their best judgment and recognize that individual actions in favor of transparency play an important role in developing norms that preserve the integrity of the community. Reviewers will be specifically instructed to not penalize honesty concerning limitations.

3. **Theory Assumptions and Proofs**

   Question: For each theoretical result, does the paper provide the full set of assumptions and a complete (and correct) proof?

   Answer: [Yes]

Justification: We provide the relevant mathematical proofs in the Appendix.

Guidelines:

- The answer NA means that the paper does not include theoretical results.
- All the theorems, formulas, and proofs in the paper should be numbered and cross-referenced.
- All assumptions should be clearly stated or referenced in the statement of any theorems.
- The proofs can either appear in the main paper or the supplemental material, but if they appear in the supplemental material, the authors are encouraged to provide a short proof sketch to provide intuition.
- Inversely, any informal proof provided in the core of the paper should be complemented by formal proofs provided in appendix or supplemental material.
- Theorems and Lemmas that the proof relies upon should be properly referenced.

4. **Experimental Result Reproducibility**

   Question: Does the paper fully disclose all the information needed to reproduce the main experimental results of the paper to the extent that it affects the main claims and/or conclusions of the paper (regardless of whether the code and data are provided or not)?

   Answer: [Yes]

   Justification: We describe the experiments in the main body and detail the implementation in the Appendix.

   Guidelines:

   - The answer NA means that the paper does not include experiments.
   - If the paper includes experiments, a No answer to this question will not be perceived well by the reviewers: Making the paper reproducible is important, regardless of whether the code and data are provided or not.
   - If the contribution is a dataset and/or model, the authors should describe the steps taken to make their results reproducible or verifiable.
   - Depending on the contribution, reproducibility can be accomplished in various ways. For example, if the contribution is a novel architecture, describing the architecture fully might suffice, or if the contribution is a specific model and empirical evaluation, it may be necessary to either make it possible for others to replicate the model with the same dataset, or provide access to the model. In general. releasing code and data is often one good way to accomplish this, but reproducibility can also be provided via detailed instructions for how to replicate the results, access to a hosted model (e.g., in the case of a large language model), releasing of a model checkpoint, or other means that are appropriate to the research performed.
   - While NeurIPS does not require releasing code, the conference does require all submissions to provide some reasonable avenue for reproducibility, which may depend on the nature of the contribution. For example
     (a) If the contribution is primarily a new algorithm, the paper should make it clear how to reproduce that algorithm.
     (b) If the contribution is primarily a new model architecture, the paper should describe the architecture clearly and fully.
     (c) If the contribution is a new model (e.g., a large language model), then there should either be a way to access this model for reproducing the results or a way to reproduce the model (e.g., with an open-source dataset or instructions for how to construct the dataset).
     (d) We recognize that reproducibility may be tricky in some cases, in which case authors are welcome to describe the particular way they provide for reproducibility. In the case of closed-source models, it may be that access to the model is limited in some way (e.g., to registered users), but it should be possible for other researchers to have some path to reproducing or verifying the results.

5. **Open access to data and code**

   Question: Does the paper provide open access to the data and code, with sufficient instructions to faithfully reproduce the main experimental results, as described in supplemental material?

Answer: [Yes]

Justification: We use open-source datasets with references for the evaluation. All code is provided in the supplementary material.

Guidelines:

- The answer NA means that paper does not include experiments requiring code.
- Please see the NeurIPS code and data submission guidelines (`https://nips.cc/public/guides/CodeSubmissionPolicy`) for more details.
- While we encourage the release of code and data, we understand that this might not be possible, so "No" is an acceptable answer. Papers cannot be rejected simply for not including code, unless this is central to the contribution (e.g., for a new open-source benchmark).
- The instructions should contain the exact command and environment needed to run to reproduce the results. See the NeurIPS code and data submission guidelines (`https://nips.cc/public/guides/CodeSubmissionPolicy`) for more details.
- The authors should provide instructions on data access and preparation, including how to access the raw data, preprocessed data, intermediate data, and generated data, etc.
- The authors should provide scripts to reproduce all experimental results for the new proposed method and baselines. If only a subset of experiments are reproducible, they should state which ones are omitted from the script and why.
- At submission time, to preserve anonymity, the authors should release anonymized versions (if applicable).
- Providing as much information as possible in supplemental material (appended to the paper) is recommended, but including URLs to data and code is permitted.

6. **Experimental Setting/Details**

   Question: Does the paper specify all the training and test details (e.g., data splits, hyperparameters, how they were chosen, type of optimizer, etc.) necessary to understand the results?

   Answer: [Yes]

   Justification: We provide all such experimental details in the Appendix. Ablation studies of hyperparameters are performed.

   Guidelines:

   - The answer NA means that the paper does not include experiments.
   - The experimental setting should be presented in the core of the paper to a level of detail that is necessary to appreciate the results and make sense of them.
   - The full details can be provided either with the code, in appendix, or as supplemental material.

7. **Experiment Statistical Significance**

   Question: Does the paper report error bars suitably and correctly defined or other appropriate information about the statistical significance of the experiments?

   Answer: [Yes]

   Justification: The main results are computed from 15 runs. Error bars are provided.

   Guidelines:

   - The answer NA means that the paper does not include experiments.
   - The authors should answer "Yes" if the results are accompanied by error bars, confidence intervals, or statistical significance tests, at least for the experiments that support the main claims of the paper.
   - The factors of variability that the error bars are capturing should be clearly stated (for example, train/test split, initialization, random drawing of some parameter, or overall run with given experimental conditions).
   - The method for calculating the error bars should be explained (closed form formula, call to a library function, bootstrap, etc.)
   - The assumptions made should be given (e.g., Normally distributed errors).

- It should be clear whether the error bar is the standard deviation or the standard error of the mean.
- It is OK to report 1-sigma error bars, but one should state it. The authors should preferably report a 2-sigma error bar than state that they have a 96% CI, if the hypothesis of Normality of errors is not verified.
- For asymmetric distributions, the authors should be careful not to show in tables or figures symmetric error bars that would yield results that are out of range (e.g. negative error rates).
- If error bars are reported in tables or plots, The authors should explain in the text how they were calculated and reference the corresponding figures or tables in the text.

8. **Experiments Compute Resources**

   Question: For each experiment, does the paper provide sufficient information on the computer resources (type of compute workers, memory, time of execution) needed to reproduce the experiments?

   Answer: [Yes]

   Justification: We provide all information about the computational resources needed in the Appendix.

   Guidelines:

   - The answer NA means that the paper does not include experiments.
   - The paper should indicate the type of compute workers CPU or GPU, internal cluster, or cloud provider, including relevant memory and storage.
   - The paper should provide the amount of compute required for each of the individual experimental runs as well as estimate the total compute.
   - The paper should disclose whether the full research project required more compute than the experiments reported in the paper (e.g., preliminary or failed experiments that didn't make it into the paper).

9. **Code Of Ethics**

   Question: Does the research conducted in the paper conform, in every respect, with the NeurIPS Code of Ethics `https://neurips.cc/public/EthicsGuidelines`?

   Answer: [Yes]

   Justification: The research conforms with the Code Of Ethics.

   Guidelines:

   - The answer NA means that the authors have not reviewed the NeurIPS Code of Ethics.
   - If the authors answer No, they should explain the special circumstances that require a deviation from the Code of Ethics.
   - The authors should make sure to preserve anonymity (e.g., if there is a special consideration due to laws or regulations in their jurisdiction).

10. **Broader Impacts**

    Question: Does the paper discuss both potential positive societal impacts and negative societal impacts of the work performed?

    Answer: [Yes]

    Justification: We discuss the broader impacts of our work in the Appendix.

    Guidelines:

    - The answer NA means that there is no societal impact of the work performed.
    - If the authors answer NA or No, they should explain why their work has no societal impact or why the paper does not address societal impact.
    - Examples of negative societal impacts include potential malicious or unintended uses (e.g., disinformation, generating fake profiles, surveillance), fairness considerations (e.g., deployment of technologies that could make decisions that unfairly impact specific groups), privacy considerations, and security considerations.

- The conference expects that many papers will be foundational research and not tied to particular applications, let alone deployments. However, if there is a direct path to any negative applications, the authors should point it out. For example, it is legitimate to point out that an improvement in the quality of generative models could be used to generate deepfakes for disinformation. On the other hand, it is not needed to point out that a generic algorithm for optimizing neural networks could enable people to train models that generate Deepfakes faster.
- The authors should consider possible harms that could arise when the technology is being used as intended and functioning correctly, harms that could arise when the technology is being used as intended but gives incorrect results, and harms following from (intentional or unintentional) misuse of the technology.
- If there are negative societal impacts, the authors could also discuss possible mitigation strategies (e.g., gated release of models, providing defenses in addition to attacks, mechanisms for monitoring misuse, mechanisms to monitor how a system learns from feedback over time, improving the efficiency and accessibility of ML).

11. **Safeguards**

    Question: Does the paper describe safeguards that have been put in place for responsible release of data or models that have a high risk for misuse (e.g., pretrained language models, image generators, or scraped datasets)?

    Answer: [NA]

    Justification: The paper focuses on uncertainty quantification in classification tasks and is evaluated on existing benchmarks. The paper poses no such risks.

    Guidelines:

    - The answer NA means that the paper poses no such risks.
    - Released models that have a high risk for misuse or dual-use should be released with necessary safeguards to allow for controlled use of the model, for example by requiring that users adhere to usage guidelines or restrictions to access the model or implementing safety filters.
    - Datasets that have been scraped from the Internet could pose safety risks. The authors should describe how they avoided releasing unsafe images.
    - We recognize that providing effective safeguards is challenging, and many papers do not require this, but we encourage authors to take this into account and make a best faith effort.

12. **Licenses for existing assets**

    Question: Are the creators or original owners of assets (e.g., code, data, models), used in the paper, properly credited and are the license and terms of use explicitly mentioned and properly respected?

    Answer: [Yes]

    Justification: We use open-source datasets with references for the experimental evaluation. We have cited all the datasets and models used in this paper.

    Guidelines:

    - The answer NA means that the paper does not use existing assets.
    - The authors should cite the original paper that produced the code package or dataset.
    - The authors should state which version of the asset is used and, if possible, include a URL.
    - The name of the license (e.g., CC-BY 4.0) should be included for each asset.
    - For scraped data from a particular source (e.g., website), the copyright and terms of service of that source should be provided.
    - If assets are released, the license, copyright information, and terms of use in the package should be provided. For popular datasets, `paperswithcode.com/datasets` has curated licenses for some datasets. Their licensing guide can help determine the license of a dataset.

- For existing datasets that are re-packaged, both the original license and the license of the derived asset (if it has changed) should be provided.
- If this information is not available online, the authors are encouraged to reach out to the asset's creators.

13. **New Assets**

    Question: Are new assets introduced in the paper well documented and is the documentation provided alongside the assets?

    Answer: [NA]

    Justification: The paper does not release new assets.

    Guidelines:

    - The answer NA means that the paper does not release new assets.
    - Researchers should communicate the details of the dataset/code/model as part of their submissions via structured templates. This includes details about training, license, limitations, etc.
    - The paper should discuss whether and how consent was obtained from people whose asset is used.
    - At submission time, remember to anonymize your assets (if applicable). You can either create an anonymized URL or include an anonymized zip file.

14. **Crowdsourcing and Research with Human Subjects**

    Question: For crowdsourcing experiments and research with human subjects, does the paper include the full text of instructions given to participants and screenshots, if applicable, as well as details about compensation (if any)?

    Answer: [NA]

    Justification: The paper does not involve crowdsourcing nor research with human subjects.

    Guidelines:

    - The answer NA means that the paper does not involve crowdsourcing nor research with human subjects.
    - Including this information in the supplemental material is fine, but if the main contribution of the paper involves human subjects, then as much detail as possible should be included in the main paper.
    - According to the NeurIPS Code of Ethics, workers involved in data collection, curation, or other labor should be paid at least the minimum wage in the country of the data collector.

15. **Institutional Review Board (IRB) Approvals or Equivalent for Research with Human Subjects**

    Question: Does the paper describe potential risks incurred by study participants, whether such risks were disclosed to the subjects, and whether Institutional Review Board (IRB) approvals (or an equivalent approval/review based on the requirements of your country or institution) were obtained?

    Answer: [NA]

    Justification: The paper does not involve crowdsourcing nor research with human subjects.

    Guidelines:

    - The answer NA means that the paper does not involve crowdsourcing nor research with human subjects.
    - Depending on the country in which research is conducted, IRB approval (or equivalent) may be required for any human subjects research. If you obtained IRB approval, you should clearly state this in the paper.
    - We recognize that the procedures for this may vary significantly between institutions and locations, and we expect authors to adhere to the NeurIPS Code of Ethics and the guidelines for their institution.
    - For initial submissions, do not include any information that would break anonymity (if applicable), such as the institution conducting the review.